Mechanical behavior at high temperature of highly oxygen- or hydrogen-enriched α and (prior-) β phases of zirconium alloys

I. Turque, R. Chosson, Matthieu Le Saux, J.-C. Brachet, V. Vandenberghe, J. Crepin, Af, Gourgues-Lorenzon

To cite this version:

I. Turque, R. Chosson, Matthieu Le Saux, J.-C. Brachet, V. Vandenberghe, et al.. Mechanical behavior at high temperature of highly oxygen- or hydrogen-enriched α and (prior-) β phases of zirconium alloys. 18th International Symposium on Zirconium in the Nuclear Industry, May 2016, Hilton Head, United States. cea-02442337

HAL Id: cea-02442337
https://cea.hal.science/cea-02442337v1

Submitted on 16 Jan 2020

I. Turque[1,2], R. Chosson[1,2,3], M. Le Saux[1], J.C. Brachet[1], V. Vandenberghe[1,4], J. Crépin[2], and A.F. Gourgues-Lorenzon[2]

Mechanical behavior at high temperature of highly oxygen- or hydrogen-enriched α and (prior-) β phases of zirconium alloys

ABSTRACT: During a hypothetical loss-of-coolant accident (LOCA), zirconium alloy fuel claddings can be loaded by internal pressure and exposed to steam at high temperature (HT, potentially up to 1200°C) until they are cooled and water quenched. A significant fraction of the oxygen reacting with the cladding during oxidation at HT diffuses beneath the oxide through the metallic substrate. This diffusion of oxygen induces a progressive transformation of the metallic β_{Zr} phase layer into an intermediate layer of $\alpha_{Zr}(O)$ phase containing up to 7 wt.% of oxygen. Furthermore, in some specific conditions, the cladding may rapidly absorb a significant amount of hydrogen during steam exposition at high temperature. Then, hydrogen, as a β_{Zr}-stabilizer, would mainly diffuse and concentrate up to several thousands of wt.ppm into the inner β_{Zr} phase layer.

It is known that oxygen and hydrogen modify the metallurgical and mechanical properties of zirconium alloys but data are scarce for high contents, especially at HT. However, such data are important basic components to improve the assessment of the oxidized cladding mechanical behavior and integrity during and after LOCA-like thermal-mechanical transients. This study intends to provide new and more comprehensive data on the mechanical behavior at HT of the $\alpha_{Zr}(O)$ and the (prior-) β_{Zr} phases containing high contents of oxygen and hydrogen, respectively. In this paper, the results of mechanical tests performed on model samples, produced from M5®[5] and Zircaloy-4 cladding tubes, homogeneously charged in oxygen (up to about 6 wt.%) or hydrogen (up to about 3000 wt.ppm) respectively, are described. The tests were performed at various temperatures under vacuum between 800 and 1100°C for the oxygen-enriched α_{Zr} phase and in air between 700 and 20°C, after cooling from the β_{Zr} temperature domain, for the hydrogen-enriched (prior-) β_{Zr} phase. The α_{Zr} phase is substantially strengthened and embrittled by oxygen. Power-law and nearly linear creep regimes are observed for stress levels beyond and below 15 MPa respectively. As confirmed by observation of fracture surfaces, the model $\alpha_{Zr}(O)$ material experiences a ductile-to-brittle transition at 1000-1100°C for oxygen contents between 3.4 and 4.3 wt.%. A model is developed to describe the viscoplastic behavior of the $\alpha_{Zr}(O)$ phase and used to evaluate the contribution of the $\alpha_{Zr}(O)$ phase layer to the creep behavior of an oxidized fuel cladding tube submitted to internal pressure at HT. Below 500°C, the model (prior-) β_{Zr} phase appears to be embrittled by hydrogen contents of 2000-3000 wt.ppm, so that it becomes macroscopically brittle at 135°C and below, and at 350-400°C, for average hydrogen contents of about 2000 wt.ppm and 3000 wt.ppm, respectively. The effect of thousands wt.ppm of hydrogen on ductility decreases with increasing temperature and vanishes beyond 500°C. When the behavior is macroscopically ductile, the (prior-) β_{Zr} phase containing between about

---

[1] CEA, DEN, DMN, Section for Applied Metallurgy Research, 91191 Gif-sur-Yvette Cedex, France, e-mail: matthieu.lesaux@cea.fr (corresponding author)

[2] MINES ParisTech, PSL Research University, Centre des matériaux, CNRS UMR 7633, BP 87, 91003 Evry, France

[3] AREVA NP, 69456 Lyon Cedex 06, France

[4] Now at CEA, DEN, DM2S, Section of Mechanical and Thermal Studies, 91191 Gif-sur-Yvette Cedex, France

[5] M5 is a trademark of AREVA NP registered in the USA and in other countries

1700 and 3200 wt.ppm of hydrogen has a higher flow stress than the material without hydrogen at 500°C and a lower one at 700°C, respectively. Young's modulus and plastic isotropy of the (prior-) β_{Zr} phase are not significantly modified by the presence of high hydrogen contents.

Keywords: Zircaloy-4, M5®, oxygen, hydrogen, LOCA, mechanical behavior, high temperature

Introduction

During a loss of coolant accident (LOCA) hypothetical scenario in a light water reactor (LWR), fuel claddings made of zirconium alloys are loaded by internal pressure and exposed to steam at high temperature (HT, up to 1200°C) before they are cooled and water quenched. Oxygen diffuses via anionic vacancies in the non-stoichiometric zirconia. At HT, a significant fraction of the oxygen that reacts at the metal/oxide interface diffuses through the metallic substrate via interstitial sites (oxygen diffusion into the metal is negligible at nominal operating temperatures, *i.e.* below 400°C). When the solubility limit of oxygen in the β_{Zr} phase is reached, a metallic layer of oxygen-stabilized α_{Zr} phase, called $\alpha_{Zr}(O)$, grows between the oxide layer and the β_{Zr} phase layer [1][2][3]. There is a strong gradient of oxygen concentration through the $\alpha_{Zr}(O)$ phase layer: the oxygen content is about 7 wt.% at the interface with the oxide layer and 2 wt.% at the interface boundary with β_{Zr}. For as-received materials and oxidation temperatures lower than or equal to 1200°C, the oxygen solubility in the β_{Zr} phase is lower than 0.6 wt.%. During cooling, the β_{Zr} phase layer transforms back into α_{Zr} and forms the so-called prior-β_{Zr} phase, with a typical Widmanstätten or parallel-lath structure morphology [4].

The cladding submitted to internal pressure at high temperature may swell and burst at the beginning of the LOCA transient. The quenching at the end of the transient induces internal stresses, due to both differences between the thermal coefficients of the different phases/layers constituting the oxidized cladding material, phases transformations, and other possible phenomena. These internal stresses, potentially associated with additional mechanical loadings, can result in a brittle failure of the cladding once it is heavily oxidized and hydrided. When analyzing the mechanical behaviour of the cladding at high temperature, and during and after quenching, both the effects of the oxygen and hydrogen should be taken into account.

On the one hand, the cladding mechanical response during a LOCA-like transient depends on its degree of oxidation. In particular, the $\alpha_{Zr}(O)$ phase layer formed at HT can have strengthening and embrittling effects [3][5][6] and a good knowledge of the mechanical properties of this phase at HT is thus an important issue. However, most of the data reported in the literature were obtained for oxygen contents lower than 2 wt.% [7][8][9][10][11][12][13] or did not concern the viscoplastic behavior at HT [7][14], so that there is no data about the creep behavior of the $\alpha_{Zr}(O)$ phase for oxygen content higher than 2 wt.%. A ductile-to-brittle transition can be drawn from the data reported in the literature as a function of the oxygen content but this transition is not known for HT and oxygen contents higher than 2 wt.%.

On the second hand, during in-service operation, a fraction of the released hydrogen due to corrosion by the water environment is absorbed by the cladding. The maximum end-of-life hydrogen content expected for high burn-up cladding is about 600 wt.ppm for Zircaloy-4 [15] and about 100 wt.ppm for M5® [16]. A significant hydrogen uptake can also occur in some specific conditions during steam exposition at high temperature. This can be for example the case under high steam pressure (as expected during an intermediate break LOCA) for Zircaloy-4 and/or in post-breakaway oxidation conditions at temperatures typically lower than 1050°C. However, the hydrogen pick-up observed under high steam pressure remains limited for the typical duration of a LOCA [17][18]. Furthermore, breakaway oxidation does not occur for oxidation times lower than at least one hour for modern nuclear fuel cladding alloys such as low-tin Zircaloy-4 and M5® [19][20][21][22], while the cladding is not expected to be exposed to steam at HT during more than a quarter of an hour during a LOCA.

"Semi-integral" LOCA tests have been performed on single unirradiated or irradiated fuel rods [23][24][25] or on a bundle of rods [26] to simulate the whole LOCA transient: heating, ballooning and burst, high temperature oxidation, cooling and final water quenching with or without additional mechanical loading. These tests have shown that a fast and substantial secondary hydriding can occur during HT steam exposure following the ballooning and burst sequence: local hydrogen concentrations up to 3000-4000 wt.ppm were measured in the vicinity of burst opening after only a few tens of seconds under steam at HT. In that case, secondary hydriding results from the oxidation of the cladding inner surface after steam has penetrated through the burst opening into the gap between the fuel pellets and the inner cladding surface. Then, local hydrogen uptake is induced by the resultant increase in hydrogen partial pressure inside the gap between the cladding and the pellets when moving away from the burst opening, due to steam starved conditions [27][28]. The resultant hydrogen distribution within the cladding tube is heterogeneous, axially as well as azimuthally [29]. Due to its thermodynamic affinity to the β_{Zr} phase, hydrogen diffuses and mainly concentrates into the inner β_{Zr} phase layer [3][30][31]. It is well-established that the mechanical behavior of the cladding during and after quenching strongly depends on the properties of the (prior-) β_{Zr} phase layer.

Depending on the characteristics of the transient, failure during or after quenching can occur at the burst location, where the cladding is the thinnest and its oxidation level is the highest, or at a few centimeters away from the burst location, where the cladding is thicker and less oxidized but most heavily hydrided [26][32]. This illustrates the embrittlement effect of hydrogen. Several studies addressed the effect of hydrogen on the resistance to quenching [25] and the post-quench mechanical properties [3][24][33][34] of zirconium alloys fuel claddings oxidized at HT. It was shown that the effect of hydrogen results from an intrinsic embrittlement mechanism [3] but also from an increase, in the presence of hydrogen, of the solubility limit of oxygen in the β_{Zr} phase [35][36][37], leading to an additional embrittlement due to higher oxygen content [1][2][3][14][20]. However, most of these studies focused on hydrogen contents lower than 1000 wt.ppm as the main purpose was to investigate the effect of pre-transient in-service hydriding. To the authors' knowledge, data on the mechanical behavior of zirconium alloys containing higher hydrogen contents and cooled from HT (two phases (α_{Zr}+ β_{Zr}) and β_{Zr} domains) are very scarce and they are limited to room temperature [33][38], while an important effect of temperature is expected.

The first part of the present work deals with the creep behavior and the failure mode at HT (between 800 and 1100°C) of the $\alpha_{Zr}(O)$ phase containing more than 2 wt.% of oxygen. A part of the results has already been presented elsewhere [39]. A model is developed on the basis of these data to describe the viscoplastic behavior of the $\alpha_{Zr}(O)$ phase. This model is then used with finite element analysis to evaluate the effect of the $\alpha_{Zr}(O)$ phase layer on the creep behavior of a fuel cladding tube submitted to an internal pressure at HT. The second part of the study focusses on the mechanical behavior between 700 and 20°C, during cooling from the β_{Zr} phase domain, of the (prior-) β_{Zr} phase and on the effect of high hydrogen contents. The effect of oxygen on the properties of the (prior-) β_{Zr} phase is not directly addressed in this paper and will be published elsewhere.

Mechanical behavior of highly oxygen-enriched α_{Zr} phase

Materials and experimental procedures

Sample preparation—In order to study the mechanical behavior of the α_{Zr}(O) phase, model oxygen-enriched α_{Zr} phase samples were elaborated from fully recrystallized M5® cladding tubes from AREVA NP (nominal outer diameter and wall thickness of about 9.5 mm and 0.57 mm, respectively). The as-received chemical composition of the material is given in Table 1. The material initially contains 0.14 wt.% of oxygen and less than 5 wt.ppm of hydrogen. Oxygen charging was performed in several steps. First, the tube samples were oxidized in steam at 1100°C in the EDGAR facility [40] in order to introduce oxygen into the material, mainly under the form of outer zirconia and intermediate α_{Zr}(O) phase layers. Oxidation durations at 1100°C depend on the targeted oxygen contents. They were evaluated by using oxidation kinetics established from results previously obtained at CEA [3][20][22][18][35]. The oxidized samples were then annealed under secondary vacuum for 3h at 1200°C in order to fully homogenize the oxygen concentration (by reduction of the oxide and diffusion of oxygen across the tube wall-thickness). Model α_{Zr} phase samples with about 2 (10), 3.2 (16), 4.3 (20) and 5.8 (26) wt.% (at.%) oxygen contents were elaborated. Homogeneity and mean contents of oxygen were measured by Electron Probe Micro Analysis (EPMA, CAMECA SX100 microprobe) with typical accuracy of ±2500 wt.ppm. The obtained mean oxygen contents almost cover the typical range of oxygen contents observed in the α_{Zr}(O) phase of claddings oxidized at HT.

TABLE 1—*Nominal chemical composition (in wt.%) of the studied materials.*

Material	Sn	Fe	Cr	Nb	O	Zr
M5®	-	0.04	-	1.0	0.14	Bal.
Zircaloy-4	1.3	0.2	0.1	-	0.13	Bal.

*Mechanical testing—*Materials with such high oxygen contents are brittle at low temperature [14]. In order to avoid sample handling at room temperature and thus make it possible to carry out mechanical testing at HT, the 265 mm long oxidized specimens were mounted on an electrical-mechanical tensile machine with a radiation furnace operating under secondary vacuum [41][42] then annealed and homogenized *in-situ* into the facility, before decreasing the temperature (at a rate of a few °C/s) down to the various target creep temperatures. The creep tests were then launched directly after the homogenization stage without going down to room temperature.

The temperature was monitored by using Pt/Pt-Rh thermocouples spot-welded at the surface of the specimen. The temperature gradient along the specimen gauge length is about 10±5°C. The sample gauge length was delimited by using two alumina rings cement-pasted onto the tube.

The axial elongation was measured during the test by using a contactless laser extensometer with a spatial resolution of 1 µm.

The tube specimens were loaded in tension along their axial direction. As done in [41], several constant load levels were successively applied to each specimen. A steady-state true strain rate was evaluated for each load level. Indeed, no or very limited primary creep was observed. The tests were performed at constant temperature between 800 and 1000°C for true axial stresses ranging from 2 to 31 MPa. A test with increasing, then decreasing load levels was carried out to check that the loading history has no significant effect on the subsequent creep behavior.

Microstructure of the model materials—Samples having experienced creep testing were observed at mid-gauge length. As illustrated in Fig. 1 and Fig. 2, the oxygen-enriched specimens are mainly composed of α_{Zr}(O) grains, enriched in oxygen and depleted in niobium and iron. Regions of untransformed β_{Zr} (or prior-β_{Zr}) phase, strongly enriched in niobium (up to 8 wt.%) and iron, and containing about 0.5±0.2 wt.% of oxygen, are also observed locally (Fig. 2). The volume fraction of this residual β_{Zr} phase is very low (less than 10%) for the lowest investigated test temperatures or the highest mean oxygen contents. It reaches about 10-15% beyond 1000°C for the material containing 2 wt.% oxygen in average. This is in accordance with results of thermodynamic equilibrium calculations carried out with the Thermocalc software using the Zircobase database [43] (Fig. 3). The residual β_{Zr} phase is expected to be present during the creep tests at HT. The oxygen content is rather homogeneous within the α_{Zr}(O) phase of model samples (Fig. 2), with the exception of the one with 5.8 wt.% of oxygen in average. In this last case, a residual oxygen content relative concentration gradient greater than 30% was measured by EPMA within the cladding wall-thickness.

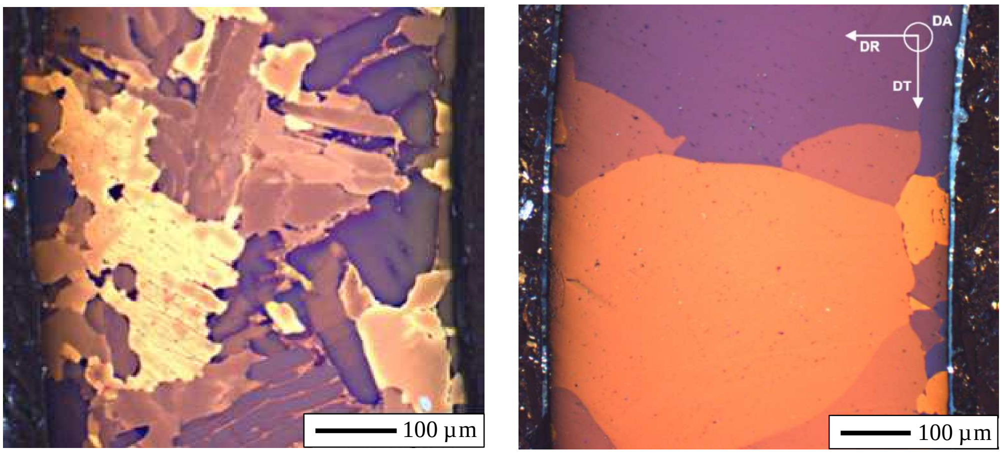

(a) (b)

FIG. 1—*Optical micrographs of transverse cross-sections of creep tested model* α_{Zr}*(O) samples containing in average (a) 2 wt.% and (b) 4.3 wt.% of oxygen (outer surface on the left); DR: radial direction; DA: tube axis; DT: circumferential direction.*

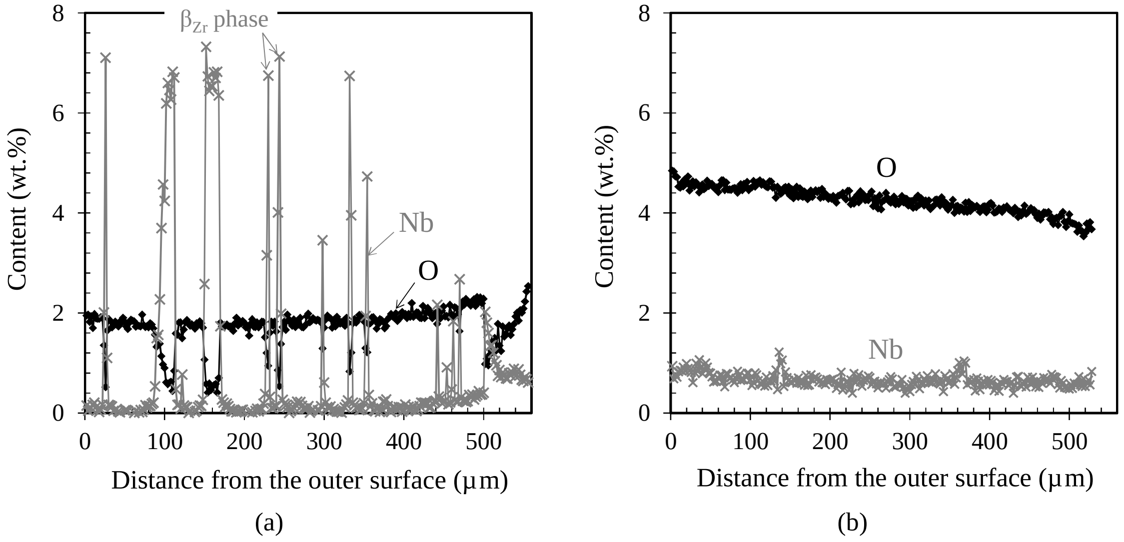

(a)

(b)

FIG. 2—*Oxygen and niobium concentration profiles (EPMA) across the thickness of model α_{Zr}(O) samples containing in average (a) 2 wt.% and (b) 4.3 wt.% of oxygen.*

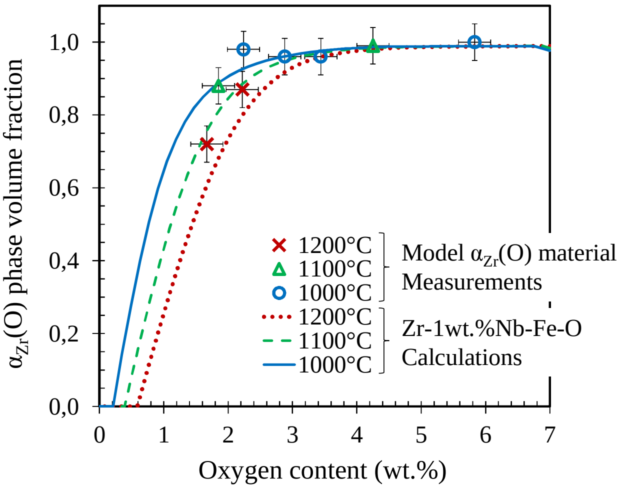

FIG. 3—*Measured (EPMA) and calculated (Thermocalc + Zircobase) α_{Zr}(O) phase volume fraction as a function of oxygen content and temperature.*

The resultant microstructure of the model material depends on the mean oxygen content (Fig. 1). In the material containing about 2 wt.% of oxygen, the α_{Zr}(O) phase morphology is characterized by coarse lamellae, mainly lying down in the tube radial-circumferential plane. These platelets have typical thickness and length ranging from 20 to 40 µm and from 100 to 200 µm, respectively. They are separated by a continuous network of residual niobium enriched prior-β_{Zr} phase and/or metastable β_{Zr} phase (in Zr-Nb alloys, due to the low thermal diffusivity of niobium and to a lower α_{Zr} transus temperature compared to Zircaloy type alloys, β_{Zr} can be stabilized due to its enrichment in niobium and can be "frozen" down to room temperature [44]). For higher oxygen contents, α_{Zr}(O) grains are more equiaxed and larger (200-500 µm) and the residual (prior-) β_{Zr} phase is not percolated. α_{Zr}(O) grains are smaller at the cladding sample surfaces. In the case of the material containing 5.8 wt.% of oxygen, a thin residual oxide layer is observed at the surface and underlying α_{Zr}(O) grains are partially columnar. Indeed, at such high oxygen content, the material is nearly saturated in oxygen (the solubility limit is about 7 wt.%) and the concentration gradient and the driving force are low, so that longer heat-treatments would have been necessary to fully homogenize the material.

The crystallographic texture of the model α_{Zr}(O) material containing a mean oxygen content of 2 wt.% was investigated by electron backscatter diffraction (EBSD) and neutron diffraction (Léon Brillouin Laboratory, CEA Saclay). Typically, about 500 grains were analyzed by EBSD, and around 10^6 by neutron diffraction. The results obtained by the two techniques, giving respectively local and overall/average information, are consistent with each other: the material exhibits a strong texture with <c> axes mainly oriented perpendicularly to the tube axis (Fig. 4). No preferential orientation of the <c> axes along the tube radial or hoop directions was evidenced by EBSD analysis (due to the tubular geometry of the sample and to the measurement procedure, radial and hoop directions could not be distinguished by neutron diffraction). Kearns factors values (defined as the fraction of resolved basal poles aligned along a particular macroscopic direction) of 0.41 and 0.44±0.05 are evaluated along the tube axial and hoop directions. This texture is comparable to that measured by EBSD for a α_{Zr}(O) layer formed during the oxidation in steam at 1100°C of a M5® cladding tube specimen (Kearns factors values of 0.36 and 0.51 along the axial and hoop directions, respectively).

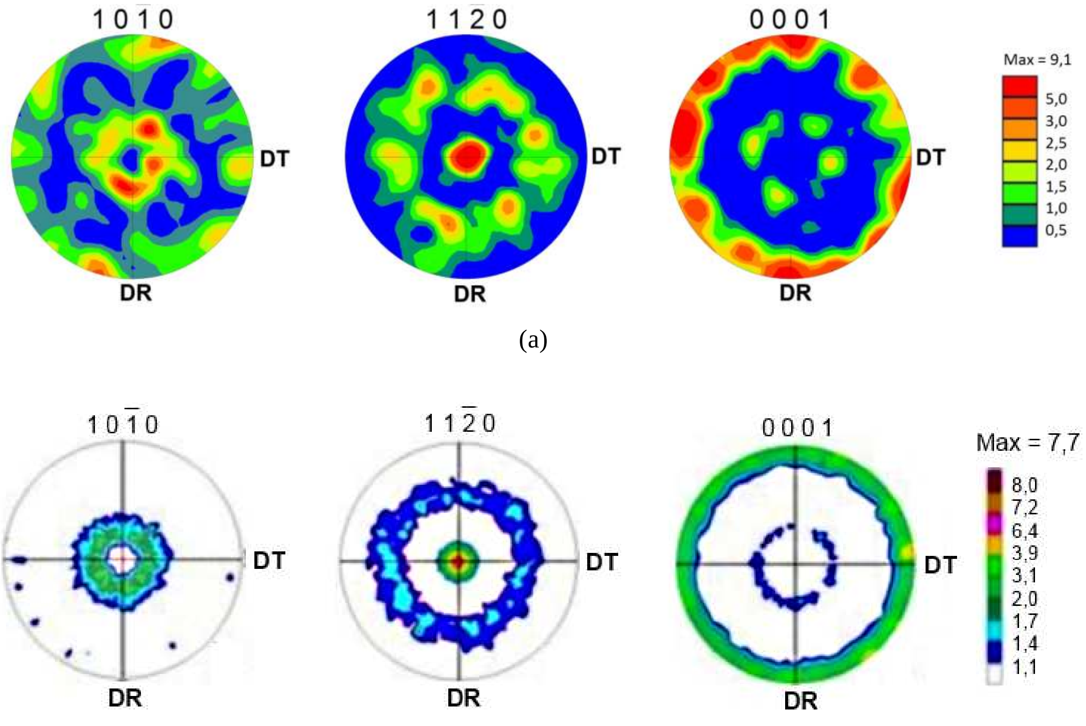

(a)

(b)

FIG. 4—*Pole figures {10.0}, {11.0} and {00.1} recalculated for a model α_{Zr}(O) sample containing 2 wt.% of oxygen in average: (a) surface analysis by EBSD, (b) volume analysis by neutron diffraction; DR: radial direction; DT: circumferential direction.*

Then, it can reasonably be considered that the model α_{Zr}(O) phase, elaborated by oxidation, dissolution and homogenization, is reasonably representative of the α_{Zr}(O) phase observed in claddings oxidized at HT [45]. However, the small volume fraction of residual β_{Zr} phase has to be taken into account for the interpretation of the tests results.

Viscoplastic behavior of the model materials

Viscoplastic flow—Results of axial tensile creep tests performed at temperatures between 800 and 1100°C on model α_{Zr}(O) samples with 2 and 3.2 wt.% of oxygen in average are shown in Fig. 5. As illustrated further down, samples with oxygen contents higher than 4 wt.% fail in a brittle manner without significant strain. Two creep regimes are observed. For stresses higher than 15 MPa, whatever the temperature between 800 and 1100°C, the behavior follows a power-law regime with a stress exponent value n close to 5. For lower stresses (lower than 10 MPa), a nearly linear flow regime is observed at 900, 1000 and 1100°C. These two creep regimes are consistent with results reported at lower temperatures for the α_{Zr} phase non-enriched in oxygen [41]. As already discussed in [39], the results confirm that the oxygen-enriched α_{Zr}(O) material has a significantly higher creep resistance than the as-received material without additional oxygen. The creep resistance increases with increasing the oxygen content. For example, the creep strain rate of the α_{Zr}(O) phase containing 2 wt.% oxygen is 10^4 times slower that rate of β_{Zr} phase, and is expected to be 100-1000 times slower than that of the α_{Zr} phase without oxygen addition. This last phase is not stable at high temperature without oxygen addition but the results presented in [41] has been extrapolated to higher temperatures for comparison to the present results. The creep rate is reduced by nearly a factor 10 when the oxygen content is increased from 2 to 2.9-3.4 wt.%.

By considering the present results for model oxygen-enriched α_{Zr}(O) phase (elaborated from M5®) and the data reported in [41] for non-oxygen enriched Zr-1wt.%Nb-0.14wt.%O, the viscoplastic strain rate of Zr-1wt.%Nb and its dependence on the oxygen content can be fairly well described by the following equation, already used by several authors (see [10], [11] and [12]):

$$\dot{\varepsilon} = \frac{A}{T} \exp\left(-\frac{Q}{RT}\right) \sigma^n \exp\left(-BC_O\right) \tag{1}$$

where $\dot{\varepsilon}$ is the true strain rate, σ is the true stress in MPa, T is the temperature in K, C_O is the oxygen content in wt.%, R is the gas constant (8.314 $\mathrm{J \cdot mol^{-1} \cdot K^{-1}}$), and A, Q, n and B are material parameters. Adjusted values of model parameters are given in Table 2 for each creep regime. The values of activation energy Q are comparable to those reported for non-oxygen enriched α_{Zr} phase in Zr-1wt.%Nb-0.14wt.%O [41]. The effect of oxygen is weaker in the linear creep regime than in the power-law creep regime. As illustrated in Fig. 5, the model accurately reproduces the behavior of the model α_{Zr}(O) phase. Nevertheless, as discussed further in the forthcoming sections, the physical deformation mechanism in the linear creep regime has not been clearly identified. As a consequence, the viscoplastic flow law tuned for this creep regime has to be considered from a phenomenological point of view only.

TABLE 2—*Model parameters adjusted to describe each regime of the viscoplastic flow of the model oxygen-enriched α_{Zr} phase.*

Strain regime	A (K.MPa^{-n}.s^{-1})	n	Q (kJ.mol^{-1})	B
Linear	$5.75\cdot10^3$	1	180	0.53
Power-law	$4.80\cdot10^3$	5	222	2.29

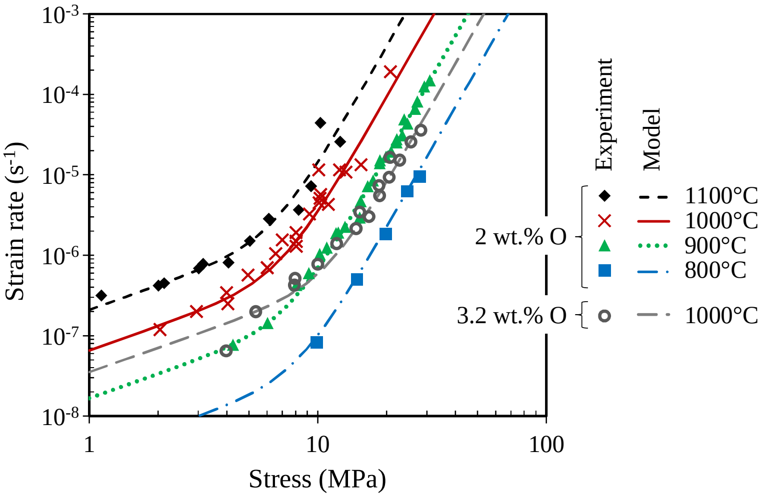

FIG. 5—*Strain rate as a function of stress: experimental data on model α_{Zr}(O) samples and predictions of the viscoplastic flow model presented in this paper.*

The predictions of this model are compared in Fig. 6 to those of models reported in the literature. The calculations were done for a temperature of 1000°C and stress levels of 2 and 20 MPa, relative to the linear and power-law creep regimes, respectively. For this purpose, models from the literature were extrapolated up to 1000°C ([10], [41] and [47]), down to 2 MPa ([10], [12] and [47]) and up to 3.2 wt.% of oxygen ([10], [12], [41] and [47])). Under a stress level of 20 MPa, the strengthening effect of oxygen predicted by the model proposed in the present paper ($B = 2.29$) is lower than those reported by Chow et al. [12] for Zircaloy-4 ($B = 2.8$) and Burton et al. [10] for Zircaloy-2 ($B = 3.42$). Oxygen contents and temperatures investigated in [12] and [10] are lower than those of the present study. Thus, the lower value obtained here for B may be due to a saturation of the strengthening effect of oxygen for contents higher than 1.5 wt.% or to a reduction of the strengthening effect with increasing temperature. For a stress level of 2 MPa, the predictions of the present model deviate significantly from those of models from the literature. This is due to the introduction of a linear creep regime, observed for the first time in a highly enriched material, the underlying physical mechanism of which still being unknown.

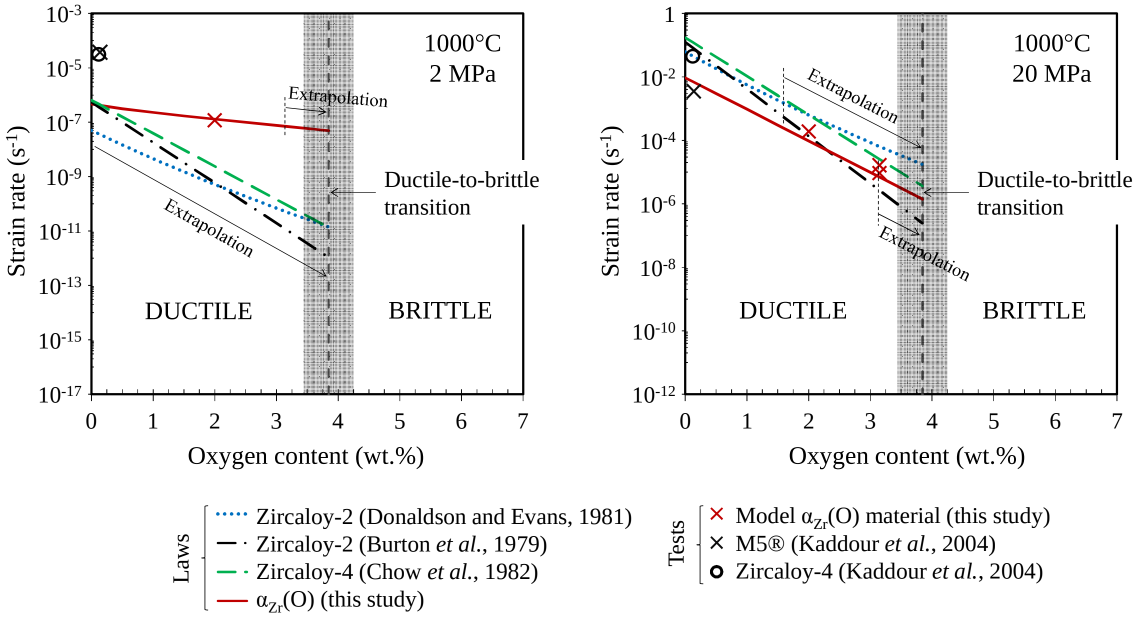

FIG. 6—*Effect of oxygen on the creep strain rate at 1000°C under 2 and 20 MPa according the creep law developed for* α_{Zr}*(O) in the present study and the laws proposed by Burton et al. [10] and Donaldson and Evans [47] for Zircaloy-2, Kaddour et al. [41] and Chow et al. [12] for Zircaloy-4 and Kaddour et al. [41] for M5®.*

Influence of microstructural features—The model oxygen-enriched material is mostly constituted of α_{Zr}(O) phase, enriched in oxygen and depleted in niobium and iron, with a minority of β_{Zr} phase, depleted in oxygen and enriched in niobium and iron. The residual fraction (up to 15%) of untransformed β_{Zr} phase is expected to have, on the one hand, a softening effect on the creep behavior of the model materials, due to the lower creep resistance of the β_{Zr} phase compared to the α_{Zr}(O) phase. On the other hand, it is expected to have a strengthening effect due to oxygen enrichment of the α_{Zr}(O) phase relatively to the mean oxygen concentration. These effects were estimated for the model material containing 2 wt.% of oxygen in average, tested above 1000°C, by using a homogenization approach with a Taylor assumption. The macroscopic axial strain rate $\dot{\mathrm{E}}$ and the axial strain rates of α_{Zr}(O) and β_{Zr} phases, respectively noted $\dot{\varepsilon}_{\alpha_{Zr}(O)}$ and $\dot{\varepsilon}_{\beta_{Zr}}$, were assumed to be equal:

$$\dot{\mathrm{E}} = \dot{\varepsilon}_{\alpha_{Zr}(O)} = \dot{\varepsilon}_{\beta_{Zr}} \tag{2}$$

The macroscopic axial stress, Σ was assumed to depend on axial stresses, $\sigma_{\alpha_{Zr}(O)}$ and $\sigma_{\beta_{Zr}}$ within α_{Zr}(O) and β_{Zr} phases, respectively, and on the volume fraction of the β_{Zr} phase, $f_{\beta_{Zr}}$:

$$\Sigma = \left(1 - f_{\beta_{Zr}}\right) \cdot \sigma_{\alpha_{Zr}(O)} + f_{\beta_{Zr}} \sigma_{\beta_{Zr}} \tag{3}$$

The mechanical behavior of the β_{Zr} phase was described by the power-law model proposed in [41] for Zr-1wt.%Nb-0.14wt.%O, modified to take into account the effect of enrichment in niobium. Trego [46] has shown that an increase in niobium content from 1 to 2.25 wt.% reduces by a factor of 0.5 the creep rate of the β_{Zr} phase. Enrichment in niobium is larger in the present case. However, in the absence of additional data, a factor 0.5 has been applied to the strain rate predicted by the model described in [41], so that the β_{Zr} phase creep rate is probably slightly overpredicted, *i.e.* the softening effect of the β_{Zr} phase is overestimated. Parameters of the power-law equation that describes the intrinsic mechanical behavior of the α_{Zr}(O) phase were then adjusted by using an iterative process so that the macroscopic response of the model for the homogenized material fits the experimental results obtained for the model α_{Zr}(O) samples (which include residual β_{Zr} phase). The results, reported in Table 3, show that the behavior of the model α_{Zr}(O) material is close to the intrinsic behavior of the α_{Zr}(O) phase: the strain rate is reduced by less than a factor 2. The strengthening effect of local enrichment in oxygen of the α_{Zr}(O) phase in the model material can be evaluated by using the model presented above (Eq. (1) and Table 2). According to predictions from this model, an increment ΔC_O of the oxygen content induces a reduction by a factor $\exp\left(-2.29\cdot\Delta C_O\right)$ of the strain rate in the power-law creep regime. The results obtained for the oxygen contents in the α_{Zr}(O) phase calculated with Thermocalc + Zircobase are given in Table 3 for the model material with a mean oxygen content of 2 wt.%. An increase in the oxygen content by 0.25 wt.% leads to a reduction of the creep rate of the α_{Zr}(O) phase by a factor 2. Thus the results show that the softening effect of the residual β_{Zr} phase and the strengthening effect of the slight enrichment in oxygen of the α_{Zr}(O) phase are relatively small (they are negligible below 1000°C and affect by a factor 2 the strain rate at 1100°C) and compensate each other in the high stress creep regime. As a consequence, these effects were not explicitly taken into account in the following. Only the values of the creep model parameters directly tuned on the basis of the data obtained on the model oxygen-enriched materials (Table 2) were used.

TABLE 3—*Estimated effects of residual β_{Zr} phase on the enrichment in oxygen of the α_{Zr}(O) phase, and on the creep rate (multiplying factors) of the model α_{Zr}(O) material with a mean oxygen content of 2 wt. %.*

	Temperature (°C)	800	900	1000	1100
	β_{Zr} phase fraction	< 0.05		0.1	0.15
	Oxygen content in α_{Zr}(O)	2-2.08		2.17	2.26
Softening due to β_{Zr} phase	Linear	< 1.1		1.1	1.2
	Power-law	< 1.3		1.9	1.9
Strengthening due to enrichment in oxygen in the α_{Zr}(O) phase	Power-law	< 1.2		1.5	1.8

Creep mechanisms in the linear regime—Beyond 1000°C and for low stress levels (< 10 MPa), a nearly linear creep regime is observed in the model material containing 2 wt.% of oxygen. In the α_{Zr} phase non-enriched in oxygen tested at lower temperatures, this linear regime is associated with a Coble type diffusion creep mechanism (diffusional flow along grain boundaries) [49]. However the grain size in the oxygen-enriched material is significantly larger (about $6.75\cdot 10^5\ \mu m^3$) than that of starting, non-enriched material (about $10^3\ \mu m^3$) and the linear creep regime may thus result from another physical viscoplastic flow mechanism. This cannot be clearly identified on the basis of available data. Nevertheless, a first qualitative analysis can be made in order to try to evaluate which among the Nabarro-Herring (bulk diffusional flow) [50], Coble and Harper-Dorn (probably dislocation core diffusion controlled) [51] creep mechanisms might significantly contribute to this flow regime.

In a first step, the effect of oxygen on these mechanisms was not taken into account. For dislocation and Coble regimes, viscoplastic flow models reported by Kaddour et al. [41] and Trego [46] were used. A grain size dependence similar to that identified in [46] was added for the Coble regime to the model described in [41]. For the Harper-Dorn and Nabarro-Herring creep regimes, no data are available for Zircaloy-4 or M5®, so that the models respectively proposed by Fiala and Cadek [52] and Prasad et al. [53] for pure zirconium were used. These last two laws probably overpredict the creep rate of zirconium alloys due to the expected effects of alloying elements. As shown in Fig. 7, at 700°C under 1 MPa, the Coble type regime prevails for grain size around 6 µm, in accordance with experimental observations. The Harper-Dorn creep predominates for grain size larger than 30-60 µm. At 1000°C, the laws were extrapolated since the α_{Zr} phase does not exist at this temperature without important addition of oxygen. According to this extrapolation, the Nabarro-Herring creep would prevail for grain sizes between 10-50 and 200 µm. This suggests that this is the main mechanism in the model material containing 2 wt.% of oxygen, which has an equivalent grain size of about 90 µm. However, the creep rates predicted by the Nabarro-Herring and Coble type creep laws are close to each other. The estimated contribution from the Harper-Dorn mechanism is the lowest at 1000°C. Thus, the Harper-Dorn mechanism is probably not the mechanism responsible for linear creep of the model oxygen-enriched material.

The $\alpha_{Zr}(O)$ phase in the model material with 2 wt.% of oxygen appears as parallel platelets with typical approximate dimensions of $30\times150\times150$ µm^3. The shorter dimension of $\alpha_{Zr}(O)$ platelets is parallel to the cladding axis, which is the tensile loading direction in the present tests. According to Nix's analysis [48], assimilating the grain to a parallelepiped, the creep rate when it is controlled by a Coble mechanism would be 2.4 times faster in a typical $\alpha_{Zr}(O)$ platelet than in a microstructure of cube-shaped grains of the same volume. The contribution of the Nabarro-Herring mechanism would not be significantly affected by the morphology of $\alpha_{Zr}(O)$ grains. It is important to note that this analysis is approximate in the present case, since the description of microstructure is very simplified. In the actual material, grain boundaries might not be perfect sources or sinks for vacancies contrary to what is assumed in Nix's model, and the actual grain distribution and the potential connection of $\alpha_{Zr}(O)$ platelets are not taken into account. However, these simple estimates suggest that the microstructure of the model material with 2 wt.% of oxygen could be more sensitive to Coble creep than to Nabarro-Herring creep in the temperature and strain rate range considered in this study.

In a second step, potential effects of oxygen were considered. It is known that oxygen has an exponential strengthening effect on the dislocation creep but to the authors' knowledge there is no data on the influence of oxygen for diffusion and Harper-Dorn mechanisms. Oxygen addition should have an important effect on the Harper-Dorn creep mechanism since this mechanism also involves dislocations, as in power-law creep regimes [54]. As a consequence, it is unlikely that the Harper-Dorn mechanism prevails in the linear creep regime. It can be imagined that oxygen interstitial atoms could have an effect on the diffusion mechanisms via their effect on the diffusion of zirconium, as observed for example for iron in zirconium [55]. No significant oxygen segregation was observed by EPMA in the model oxygen-enriched materials but the spatial resolution was not sufficient to address grain boundary segregation. Another difficulty in the present case, implying oxygen concentrations higher than 10 at.%, is that the interactions between oxygen atoms probably play a role on the diffusion mechanisms.

To conclude, with the current knowledge it appears to be difficult to identify the mechanism that drives the low-stress linear creep regime of oxygen-enriched material at HT. It is possible that the diffusion Nabarro-Herring or Coble type creep mechanisms dominate in spite of the relatively large grain size. A way to rank Nabarro-Herring, Coble and Harper-Dorn mechanisms would be to carry out tests on materials with the same oxygen content but various grain sizes.

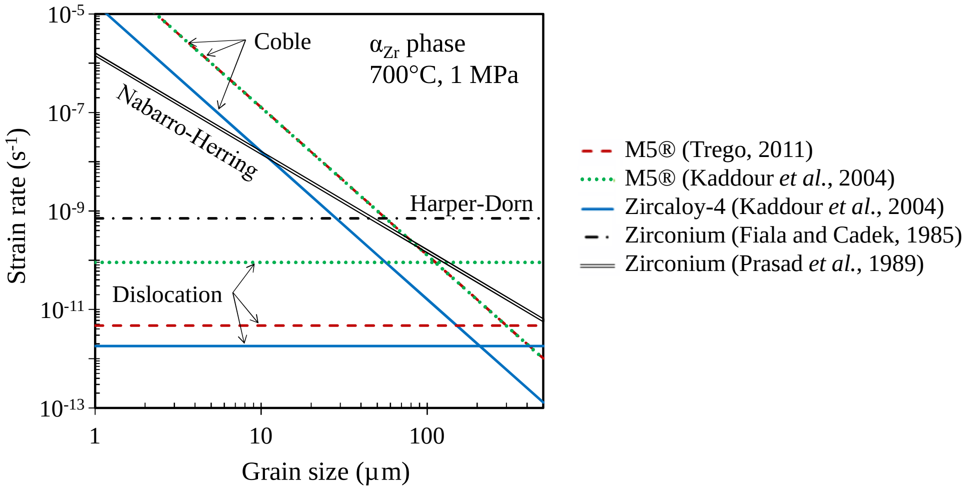

FIG. 7—*Strain rate as a function of the grain size in zirconium and its alloys according to creep models associated with diffusional flow (Coble, Nabarro-Herring), dislocation-driven and Harper-Dorn deformation mechanisms at 700°C.*

Fracture of the model materials

Macroscopic ductility—The maximal axial strain values measured during the axial tensile creep tests are reported in Fig. 8. These values are lower bounds of the actual strain values at failure. Indeed, most of the time, the alumina rings that delimit the sample gauge length fell when the axial strain reaches 4 to 10 %, so that the sample continues to deform until fracture but with no axial strain monitoring. From Fig. 8, model α_{Zr}(O) materials with oxygen contents between 2 and 3.2 wt.% are ductile between 800 and 1100°C: axial strain levels higher than 10% or even 20% are reached without failure. Samples with oxygen contents higher than 4 wt.% failed in a brittle manner, for very low strain levels, even at 1100°C. A ductile-to-brittle transition is thus highlighted at 1000-1100°C for oxygen contents between 3.4 and 4.3 wt.%.

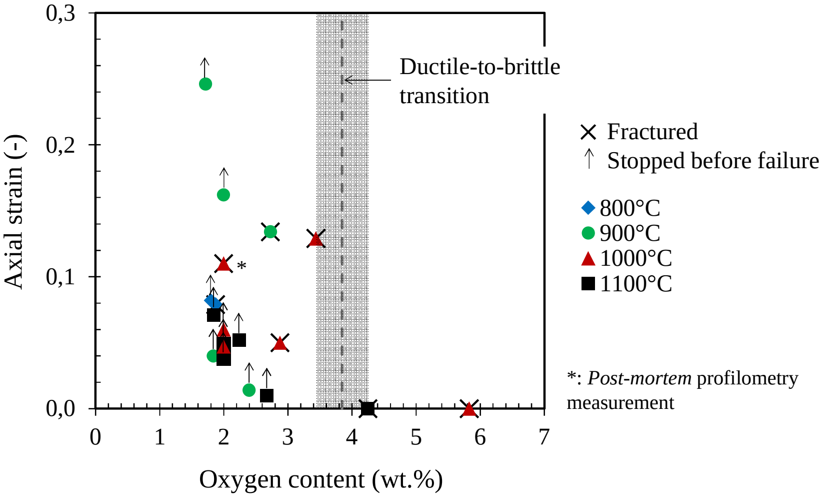

FIG. 8—*Evolution of the maximal measured axial strain (lower bound of fracture strain) as a function of the oxygen content and test temperature of the* α_{Zr}*(O) samples tested under tensile creep.*

Microscopic fracture modes—The observation by Scanning Electron Microscopy (SEM) of the fracture surfaces of creep specimens with 2 and 3.4 wt.% of oxygen shows that the fracture mode is not the same at the outer periphery and within the rest of the sample (Fig. 9). This highlights an effect of the oxidation then homogenization processing route used to elaborate the model materials: the mechanical behavior of the α_{Zr}(O) phase is different in regions where the oxide and the α_{Zr}(O) phase were located after oxidation and in regions where the α_{Zr}(O) phase was formed during the reduction/diffusion heat treatment, whereas the microstructure (chemical partitioning, texture and grain morphology) of the material in these regions could not be differentiated from that of the rest of the cladding. This difference may be due to the existence of finer and disoriented subgrains linked to the structure of the parent oxide phase layer, to a short-range ordering for particular oxygen concentration ranges and/or to defects (cavities, microcracks, …) resulting from the transformation, associated with a significant volume decrease (about 50%), of zirconia to α_{Zr}(O).

At the outer periphery of the samples, the macroscopic fracture surface is nearly perpendicular to the loading direction and suggests a nearly brittle failure mode. A network of steps, oriented along a reduced number of directions, is evidenced on the surface of these outer cracks. These steps could be due to slip along the cleavage or gliding planes of the crystals. With the exception of the sample outer periphery, an important reduction in thickness, up to almost 100% at the failure location, is measured for samples with 2 and 3.4 wt.% of oxygen. Large (> 20 µm) elliptical dimples are also observed locally on the fracture surfaces. The observation of a longitudinal cross-section of a sample containing 2 wt.% of oxygen fractured at 900°C revealed that the α_{Zr}(O) phase can withstand high strain levels. Due to its much lower oxygen content, the (prior-) β_{Zr} phase, which forms a nearly continuous network in the model material enriched to 2 wt.% of oxygen, has probably an influence on strain accommodation and strain incompatibility between α_{Zr}(O) platelets, leading to a higher macroscopic ductility. Steps similar to those observed in the nearly brittle outer zones are present on the sides and at bottom of dimples (Fig. 9(a)). The presence of these steps on the sides of dimples suggests that they are slip steps rather than cleavage steps. Steps form angles of 90 and 120°, in accordance with slip planes of the α_{Zr} phase hexagonal structure.

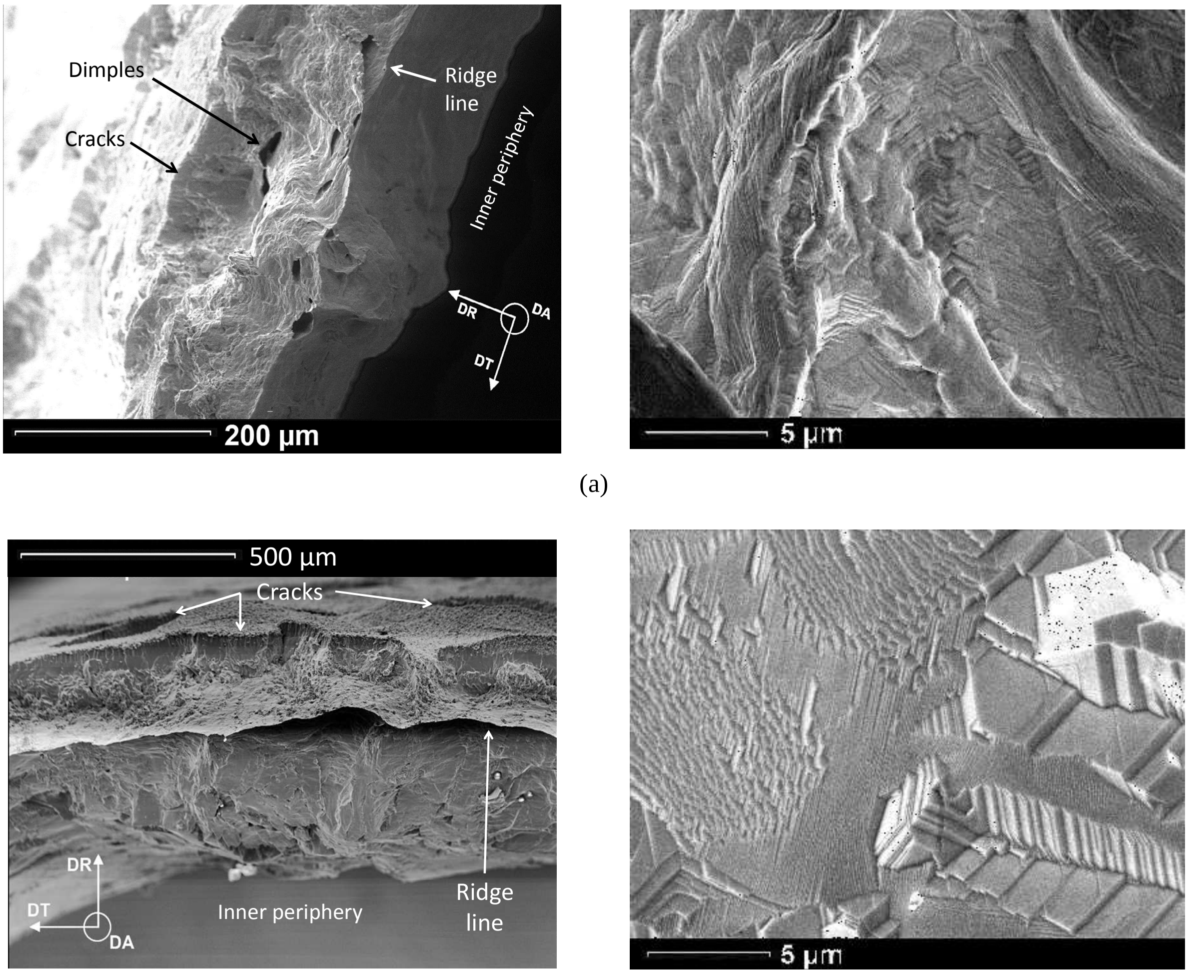

(a)

(b)

FIG. 9—*SEM micrographs of the fracture surfaces of* α_{Zr}*(O) samples containing (a) 2 wt.% of oxygen (right figure: enlarged view inside a dimple) and (b) 3.4 wt.% of oxygen (right figure: enlarged view on a nearly brittle zone) fractured at 1000°C; DR: radial direction; DA: tube axis; DT: circumferential direction.*

Model materials with 4.3 and 5.8 wt.% of oxygen exhibited a purely brittle behavior above 1000°C. For 4.3 wt.% of oxygen, grains were very coarse and fracture was mainly intergranular (Fig. 10(a)). A 50-µm-thick layer of α_{Zr}(O) phase (confirmed by EPMA) with an atypical columnar morphology was observed at the sample outer periphery. This further suggests that the initial microstructure of the oxidized material was not completely “erased” during the reduction/diffusion heat treatment under vacuum at high temperature, so that a fraction of the α_{Zr}(O) phase formed at the initial location of the prior oxide layer would have kept a columnar (sub)structure morphology. This microstructural inheritance has still to be characterized. It is thus difficult to evaluate the particular role of this layer with a specific microstructure on the overall cladding fracture mode. In the material with 5.8 wt.% of oxygen, fracture occurs mainly by cleavage and river patterns are observed on the fracture surface (Fig. 10(b)). In some regions with a flat and smooth appearance, it is not clear whether failure is intergranular or due to cleavage in a coarse grain. A thin residual columnar zirconia layer, showing an intergranular failure mode, is observed at the cladding outer periphery. The mixed cleavage and intergranular fracture mode observed at high temperature when the material is completely brittle (oxygen content higher than 4.3 wt.%) is consistent with the fracture modes reported for example by Garde et al. [56] for Zircaloy-4 with 2.3 wt.% of oxygen tested at 850°C.

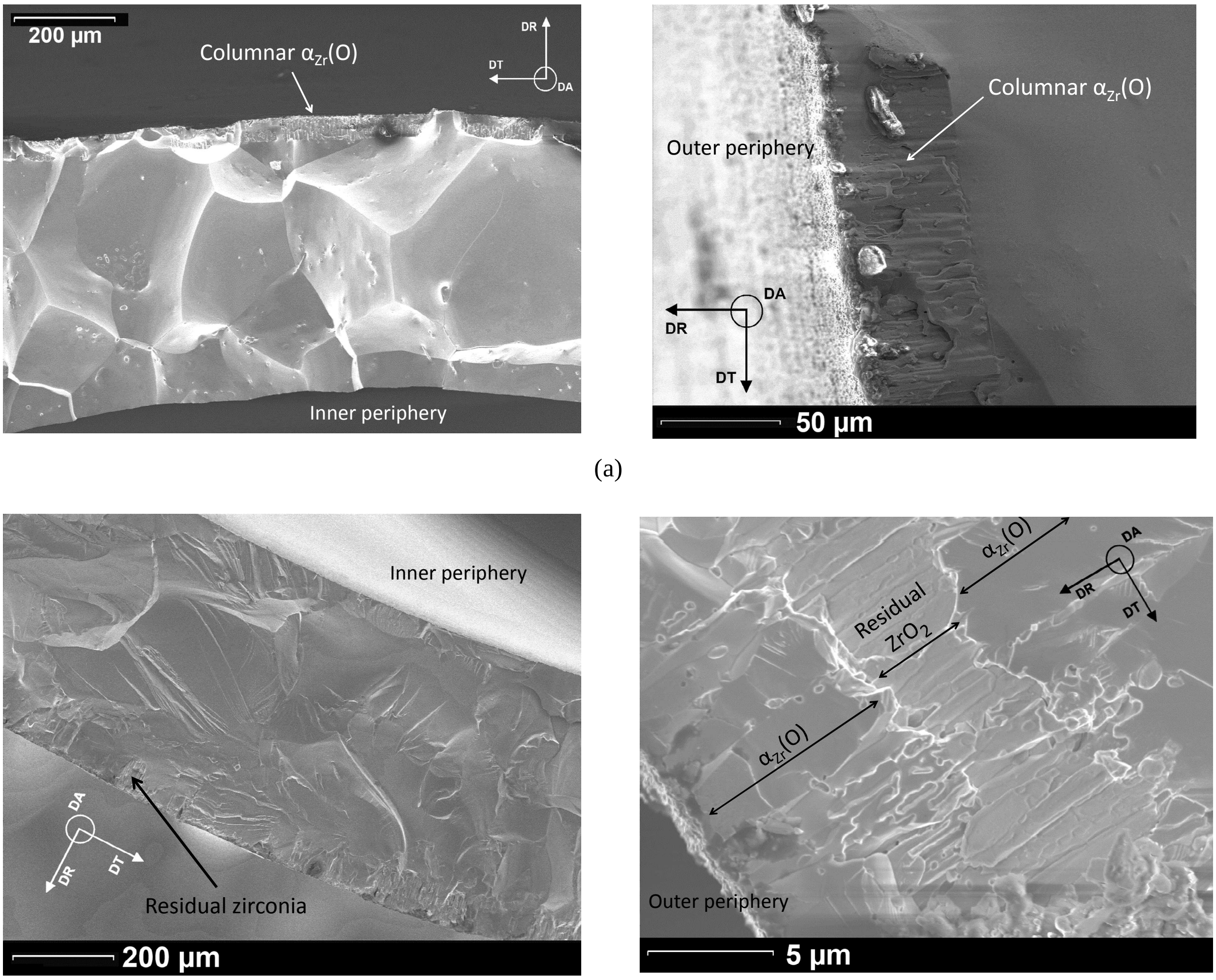

FIG. 10—*SEM micrographs of the fracture surfaces of (a) an α_{Zr}(O) sample containing 3.4 wt.% of oxygen fractured at 1100°C (right image: detailed view of α_{Zr}(O) on the tube external periphery) and (b) an α_{Zr}(O) sample containing 5.8 wt.% of oxygen fractured at 1000°C (right image: enlarged view of residual zirconia within the α_{Zr}(O) layer).*

Modeling of the creep behavior at high temperature of an oxidized cladding

Model description—In order to understand the strengthening effect of oxidation on the creep behavior of fuel cladding at high temperature, a model based on the finite element method was implemented into the finite element code Cast3M developed at CEA[6]. The purpose was to calculate the mechanical response of an oxidized cladding submitted to internal pressure creep at high temperature (1000 and 1100°C) and to compare the predictions to the results of tests performed in a steam environment in the EDGAR facility [40] on Zircaloy-4 and M5® cladding specimens.

The oxidized cladding was represented as a stratified material including three layers in the case of a one-side oxidation from the outer surface: an outer oxide layer, an $\alpha_{Zr}(O)$ phase layer and an inner β_{Zr} phase layer. In a first approach, mechanical properties were assumed to be isotropic, growth of the oxide and $\alpha_{Zr}(O)$ phase layers was not simulated so that calculations were done for predetermined constant layers thicknesses, damage or cracking were not simulated, the various layers were supposed to be perfectly adherent and separated by flat interfaces, and oxidation-induced internal stresses, thermal strains and strains due to phase transformations as well as oxide growth or oxygen ingress into the metal were not considered. The results presented in the present paper have shown that the $\alpha_{Zr}(O)$ phase is brittle at high temperature when its oxygen content exceeds about 4 wt.%. Thus it can be reasonably expected that in an oxidized cladding, the part of the $\alpha_{Zr}(O)$ phase layer that contains the highest oxygen content cracks at the very beginning of loading during a creep tensile test at high temperature. It was difficult to say from *post-mortem* observations of tested specimens whether the oxide layer fails in a brittle manner at the beginning of the test or not. Three configurations were thus considered in the simulations:

- two layers ($\beta_{Zr} + \alpha_{Zr}(O)_{2\text{-}4}$): the $\alpha_{Zr}(O)$ phase layer was considered in addition to the β_{Zr} phase layer but only that part where the oxygen content was lower than 4 wt.%;
- two layers ($\beta_{Zr} + \alpha_{Zr}(O)_{2\text{-}7}$): the β_{Zr} phase layer and the whole $\alpha_{Zr}(O)$ phase layer were considered;
- three layers ($\beta_{Zr} + \alpha_{Zr}(O)_{2\text{-}7} + ZrO_2$): the whole β_{Zr} phase, $\alpha_{Zr}(O)$ phase and oxide layers were taken into account.

The simulations were performed in 3D although they could have been carried out in 2D. A small portion (0.02° sector with a height of 2 µm) of the cladding was meshed by using quadratic brick elements with full integration. The size along the tube radial direction of the elements within the $\alpha_{Zr}(O)$ and oxide layers was 1 or 2 µm according to whether the thickness of the layers was lower than 10 µm or not. A varying mesh density was defined for the β_{Zr} phase layer: the element thickness was similar to the one used for the $\alpha_{Zr}(O)$ layer next to this last layer and was larger (20 µm) near the inner tube surface. The thicknesses of the oxide and $\alpha_{Zr}(O)$ phase layers were evaluated from growth kinetics determined on the basis of data obtained at CEA on samples oxidized in steam at high temperature [3][18][35]. The oxygen content distribution throughout the oxidized cladding was represented by introducing an oxygen concentration field defined at Gauss points. A linear oxygen concentration gradient was defined across the $\alpha_{Zr}(O)$ phase layer (from 2 wt.% at the interface with the β_{Zr} layer to 4 or 7 wt.% at the opposite surface, according to the selected configuration). Arbitrary, but reasonable oxygen contents were defined for the β_{Zr} phase and the oxide, as the oxygen content does not have a significant effect on the mechanical behavior of the first one and is not useful to describe the behavior of the second one.

---

[6] http://www-cast3m.cea.fr/

Standard symmetry conditions were applied to the nodes of the upper, lower and lateral surfaces. From a preliminary study of specimens subjected to internal pressure creep, zero displacement imposed along the tube axial direction was representative of the mechanical response of an isotropic cladding material submitted to a closed-end internal pressurization test. An internal pressure, updated at each time-step in order to account for the deformed geometry, was applied to the tube inner surface. The calculations were performed by using an updated Lagrangian method. A variable time-step between 0.1 and 200s was used for the investigated range of creep rates (10^{-2}-10^{-8} s^{-1}). It was checked that the mesh sizes and the time-steps used were small enough to guarantee that the results were not significantly affected by the spatial and temporal discretization.

The total strain was additively decomposed into elastic and viscoplastic strains (the stress threshold value between elastic and viscoplastic regimes was set to zero). Elastic strains were calculated via a isotropic Hooke's law with Young's modulus values of 44 GPa for β_{Zr} and $\alpha_{Zr}(O)$ phases and 200 GPa for zirconia, and a Poisson's ratio value of 0.3 for all the phases. By assuming that linear and power-law creep regimes coexist although one or the other dominates depending on the condition, the viscoplastic strain rate tensor was defined as the sum of the viscoplastic strain rate tensors corresponding to each of the two creep regimes. Each viscoplastic strain rate tensor was obtained by assuming the normality rule. It was considered that the two viscoplastic strain rates were associated with the same flow direction. Although the material was anisotropic and textured, a von Mises equivalent stress was used. The plastic multipliers were given for each regime by the viscoplastic flow equations in the form of Eq. (1). The viscoplastic behavior of the β_{Zr} phase was described by the flow equation proposed in [41] for Zircaloy-4 and by those presented in [41] and [46] for M5®. The flow equation described in the present paper (Eq. (1) and Table 2) was used to describe the oxygen-dependent viscoplastic behavior of the $\alpha_{Zr}(O)$ phase. The viscoplastic behavior of the oxide layer was not known at high temperature. In a first approach, the viscoplastic behavior of the oxide was described by a power-law equation tuned on the basis of results of creep compression tests performed at high temperature on a bulk, industrial doped monoclinic and tetragonal zirconia [57][58][59]; the following adjusted values were found for parameters in Eq. (1): $A = 5.08 \cdot 10^{15}$ $K.MPa^{-n}.s^{-1}$, $n = 1.52$, $Q = 500$ $kJ.mol^{-1}$, $B = 0$. According to these data, the creep rate of zirconia for a given stress is within the range of the rates expected for the $\alpha_{Zr}(O)$ phase, which contains 2 to 7 wt.% of oxygen. This law provides certainly a very rough representation of the behavior of the oxide layer of interest here, whose chemical composition and microstructure are very different from those of industrial doped zirconia.

Results and discussion—As shown in Fig. 11, the ($\beta_{Zr} + \alpha_{Zr}(O)_{2\text{-}4}$) model significantly underestimates (by a factor 100 to 1000) the gradual reduction in strain rate observed during internal pressure creep tests performed under steam at high temperature. The experimental results are fairly well reproduced by the ($\beta_{Zr} + \alpha_{Zr}(O)_{2\text{-}7}$) model. The supplementary strengthening brought by the addition of the oxide layer (($\beta_{Zr} + \alpha_{Zr}(O)_{2\text{-}7} + ZrO_2$) model) is limited (factor 2 on the creep rate). In that case, the creep resistance of the cladding is slightly overpredicted. The conclusions are similar for all the other conditions tested, for Zircaloy-4 and M5® claddings and creep temperatures of 1000 and 1100°C. This suggests *a posteriori* that the

$\alpha_{Zr}(O)$ phases formed in Zircaloy-4 and M5® have comparable microstructures and mechanical behaviors.

The deformation mechanism associated with the linear creep regime of the $\alpha_{Zr}(O)$ phase was not clearly identified and it was not possible to determine whether it is sensitive to the grain size or not. As a consequence, the flow equation proposed to describe the viscoplastic behavior of the $\alpha_{Zr}(O)$ phase does not account for an eventual grain size effect. In order to evaluate the impact of this assumption on the results, the creep law of the $\alpha_{Zr}(O)$ phase in the linear regime was modified by adding a cubic dependence on the grain size (Coble type diffusion creep). A reference grain size of 66 µm was chosen in accordance with the analysis made above. A grain size equal to the thickness of the $\alpha_{Zr}(O)$ layer (2-70 µm) is considered. The results obtained with the (β_{Zr} + $\alpha_{Zr}(O)_{2\text{-}7}$) model are only slightly modified by the introduction of this grain size dependence, which therefore does not question the main conclusions of this study.

The calculations show that it is necessary to consider that the $\alpha_{Zr}(O)$ phase is not cracked, even partially, to correctly predict the mechanical behavior of the oxidized cladding. This is in contradiction with fractographic results from the present study. This mechanical strength is all the more surprising as simulations predict high stress levels (up to about 200 MPa) in the outer part of the $\alpha_{Zr}(O)$ layer in oxidized claddings submitted to creep tests. This discrepancy could be due, for instance, to the following effects, which were not taken into account in the simulations: internal stresses generated by the oxidation, anisotropy of the $\alpha_{Zr}(O)$ and zirconia mechanical properties and/or interaction between oxidation and viscoplastic deformation.

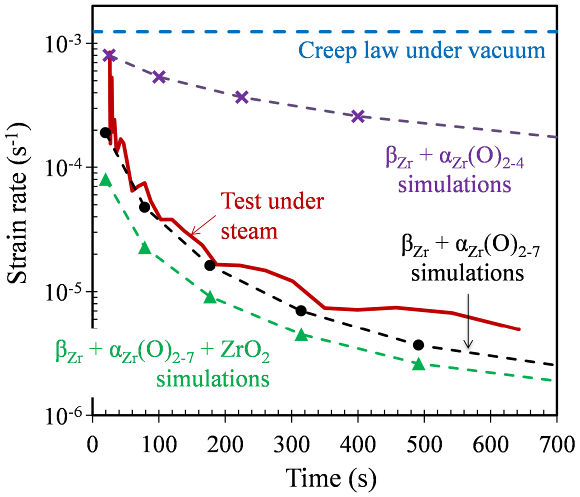

FIG. 11—*Evolution of the creep strain rate during an internal pressure creep test performed on a Zircaloy-4 cladding specimen in steam at 1100°C with a 5 bar internal pressure: experimental result, prediction of the creep model presented in [41] for a non-oxidized cladding and results of finite element simulations considering two or three layers.*

Partial conclusion

The mechanical behavior of the $\alpha_{Zr}(O)$ phase at HT was investigated through axial tensile creep tests performed under vacuum between 800 and 1100°C on model materials, elaborated from

M5® cladding, homogeneously enriched in oxygen at various contents between 2 and 5.8 wt.%. It was shown that the α_{Zr} phase is significantly strengthened and embrittled by oxygen. Two creep regimes were observed depending on stress level. Creep and failure mechanisms have been discussed. A ductile-to-brittle transition was observed at 1000-1100°C for oxygen contents between 3.4 and 4.3 wt.%. The contribution of the α_{Zr}(O) phase layer to the creep behavior of an oxidized fuel cladding tube submitted to internal pressure at HT was evaluated by finite element analysis.

Mechanical behavior of the highly hydrogen-enriched (prior-) β_{Zr} phase

Materials and experimental procedures

Sample preparation—In order to study the effect of high hydrogen contents (up to about 3200 wt.ppm) on the mechanical properties of the (prior-) β_{Zr} phase, model hydrogen-enriched samples were produced from as-received stress-relieved annealed low tin Zircaloy-4 cladding tubes (outer diameter and thickness of about 9.5 mm and 0.57 mm, respectively) supplied by AREVA NP. The as-received material chemical composition is given in Table 1. The material initially contains about 0.13 wt.% of oxygen and less than 5 wt.ppm of hydrogen. 60-mm-long cladding tube samples were charged in hydrogen by gaseous charging at 800°C in a furnace in a flowing mixture of argon and hydrogen and were then cooled down to room temperature at a rate of a few °C/min.

The hydrogen content was measured for each sample by using an inert gas fusion thermal conductivity technique (various analyzers were used: HORIBA EMGA-821, HORIBA EMGA-921, LECO RH404). Hydrogen content measurements were also performed on a selected number of samples by differential scanning calorimetry, micro elastic recoil detection analysis (μ-ERDA) (CEA Saclay, DSM, IRAMIS, SIS2M, LEEL) [30][31] and neutron radiography (CEA Saclay, DEN, DRSN, SEROS). The relative uncertainty on hydrogen content measurement is estimated to be about ±15% for the highest hydrogen contents investigated here. The measured hydrogen contents range from about 1700 to 3200 wt. ppm. It was checked that homogeneity of hydrogen content within the samples is satisfactory for the present application. Infrared absorption analyses (LECO TC500 analyzer) have shown that a slight oxygen uptake of about 0.07±0.02 wt.% occurs during the hydrogen charging treatment, so that hydrogen-charged samples contain about 0.21±0.01 wt.% of oxygen on average, instead of 0.13 wt.% in the as-received material.

Microstructure of the model materials right after hydrogen charging—The purpose of this part of the study was to characterize the properties of the β_{Zr} phase. As a consequence, a heat-treatment in the β_{Zr} phase domain has been applied to the samples before mechanical testing. However, it is interesting to briefly discuss the evolution of the material during hydrogen charging by looking at the material microstructure right after hydrogen charging. Observations by optical microscopy and SEM and chemical micro-analysis by EPMA performed on a selected number of samples did not evidence any oxide layer. However, thin layers of α_{Zr}(O) phase enriched in oxygen were observed at the sample surfaces, in accordance with the above mentioned slight oxygen uptake.

The material microstructure right after hydrogen-charging depends on the mean hydrogen content. At 800°C, the as-received material is in the α_{Zr} phase. During hydrogen-charging at 800°C, once the hydrogen content is high enough, the primary α_{Zr} phase progressively transforms into the β_{Zr} phase due to the effect of hydrogen on the phase transformation temperatures. For hydrogen contents of 2000 and 3000 wt.ppm, the material is expected to have fully transformed into β_{Zr} phase at 800°C. As illustrated in Fig. 12, at the beginning of cooling, above the eutectoid temperature (about 550°C [43]), the β_{Zr} phase progressively transforms into proeutectoid α_{Zr} phase. The eutectoid reaction then leads to a fast transformation of the residual β_{Zr} grains into α_{Zr} grains. As a consequence, the material right after hydrogen-charging at 800°C up to about 2000 and 3000 wt.ppm is constituted of a mixture of proeutectoid α_{Zr} phase and α_{Zr} phase that appeared below the eutectoid temperature (corresponding respectively to the lightest and darkest regions in Fig. 12(a)). As a result of element partitioning, the first one is enriched in α_{Zr}-stabilizers (oxygen in particular) and depleted in β_{Zr}-stabilizers (hydrogen in particular) and the second one is depleted in α_{Zr}-stabilizers and enriched in β_{Zr}-stabilizers. As exemplified in Fig. 12, according to thermodynamic calculations performed with the Thermocalc software using the Zircobase database [43], the β_{Zr} phase volume fractions just before the eutectoid transformation (at equilibrium) are about 45 and 65% for the materials containing respectively 2000 and 3000 wt.ppm of hydrogen in average. This is in accordance with the microstructures observed right after hydrogen-charging.

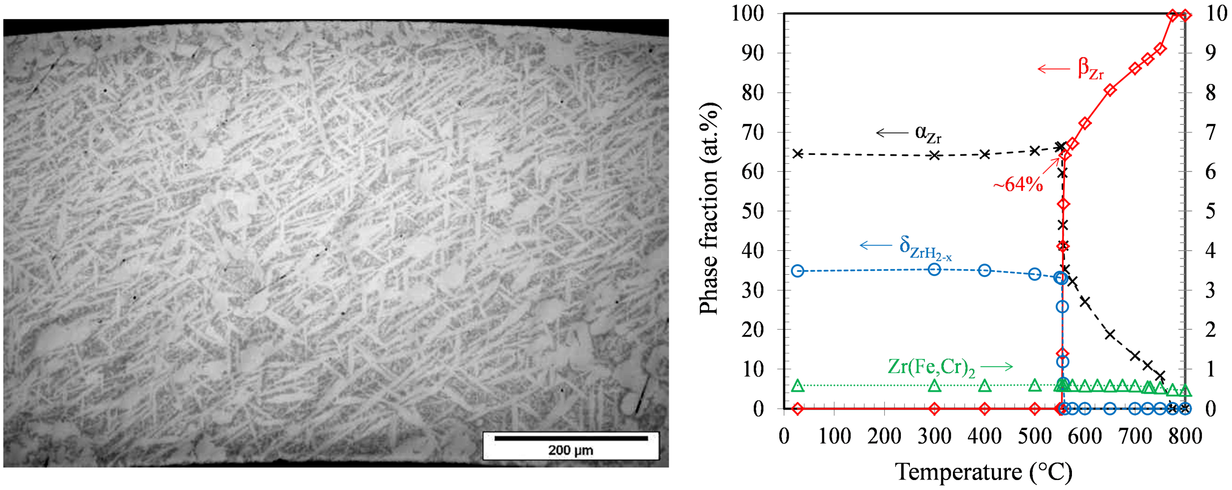

(a) (b)

FIG. 12—*(a) Optical micrograph of a transverse cross-section right after hydrogen-charging at 800°C (and cooling at a few °C/min) of a Zircaloy-4 sample containing about 3200 wt.ppm of hydrogen (and about 0.2 wt.% of oxygen) and (b) calculated (Thermocalc + Zircobase) evolution of equilibrium phases volume fractions for Zircaloy-4 containing 3000 wt.ppm of hydrogen (and 0.14 wt.% of oxygen) as a function of temperature.*

Mechanical testing—Uniaxial tensile test specimens with a gauge length of 8 mm and a gauge width of 2 mm (Fig. 13) were fabricated from the cladding tubes, hydrided or not. For each specimen, oxygen and hydrogen contents were measured respectively by infrared absorption (LECO TC500 analyzer) and thermal conductivity (LECO TC500 and HORIBA EMGA-921 analyzers) from the offcuts on both sides of the gauge length.

The specimens were mounted on an electrical-mechanical tensile machine with a radiation furnace. They were then quickly heat-treated in the β_{Zr} temperature domain (heating at about 15°C/s up to 800°C then about 3°C/s up to approximately 1200°C) into the facility and almost directly cooled (*i.e.* holding of only a few tens of seconds at HT) afterwards by turning off the power to the furnace, down to the target temperature for the tensile test, which was then directly launched. The cooling rate is about 5°C/s between 1200°C and 700°C, 1°C/s around 500°C and lower than 1°C/s below. The tests were performed upon cooling from the β_{Zr} temperature domain and not after cooling and reheating to the test temperature to guarantee that the microstructure and thus the mechanical behavior of the material are representative of those of the (prior-) β_{Zr} phase during cooling and quenching at the end of a LOCA-type transient. Temperatures of tensile tests between 700 and 20°C were investigated. The temperature was monitored by using three Pt/Pt-Rh thermocouples spot-welded at the surface of the specimen holding device. A thermal benchmark was performed beforehand to set the temperature monitoring by comparison to the targeted test temperatures. The temperature gradient along the specimen gauge length and the temperature uncertainty and variation during the tests were expected to be lower than 10°C, respectively. The tests were performed in air so that a thin oxide layer (thickness of about 5-10 µm) grows during heating at the specimen surfaces in order to prevent hydrogen desorption. A thin α_{Zr}(O) layer (thickness of about 5-10 µm) also formed beneath the oxide layer and a limited amount of oxygen could have diffused into the β_{Zr} phase. The effect on the results of this slight oxidation is discussed later in the paper. The tests were performed with a constant displacement rate of 0.8 $mm \cdot s^{-1}$ so that the mean strain rate was about 0.1 s^{-1}. By applying this relatively fast strain rate, metallurgical evolutions and oxidation of the material during the test were minimized. This loading rate is expected to be faster than the rates at which the cladding can be submitted during a LOCA transient.

In order to characterize the Young's modulus and plastic strain anisotropy, axial elongation and width reduction of the specimen gauge part were measured during the experiments before necking by using a 2D digital image correlation technique (optical method that provides local displacement and strain fields on the surface of the observed object by comparing digital images of a reference and a deformed configuration). The patterns that offer the local contrast required for the identification of homologous points were obtained by marking the outer surface of the specimen gauge part with a titanium dioxide based white fluid. The surface to analyze was illuminated in white light and observed by an optical camera with an image rate of 250 images per second. The VIC-2D™[7] software was used for the digital image correlation. Axial and hoop strains fields measured along specimen length and width were averaged over the specimen gauge part. An accuracy better than $\pm 3 \cdot 10^{-4}$ is expected on mean strain measurements.

Engineering stress was calculated by dividing the applied force by the specimen initial cross-section. Parameters representative of tensile tests, such as yield stress at 0.2% plastic strain, ultimate stress (maximum stress value measured during the test) and uniform elongation (plastic strain at the maximum stress, corresponding to the onset of necking in the case of ductile materials), were determined from engineering stress-strain curves, with the engineering strain being calculated by dividing the cross-head displacement by the specimen initial gauge length. The engineering axial strain measured by digital image correlation was used for the evaluation of

---

[7] VIC-2D is a trademark of Correlated Solutions, Inc.

Young's modulus. In order to characterize the ductility of the material, the cross-section reduction at failure was optically measured after fracture of the specimens (observations performed parallel to the tensile axis) with an absolute accuracy of about ±8%.

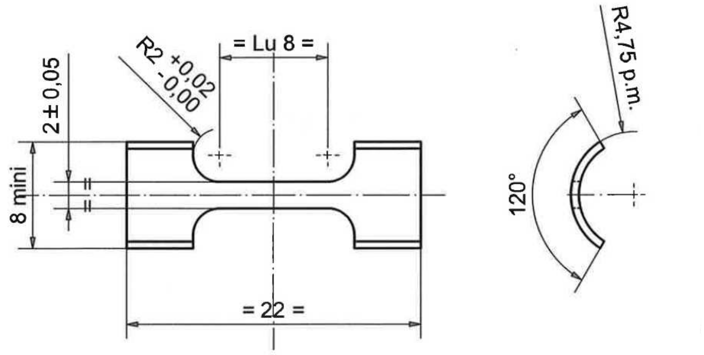

FIG. 13—*Specimen used for axial tensile tests on (prior-)* β_{Zr} *materials (dimensions in mm).*

Results and discussion

Elasticity—As illustrated in Fig. 14, the value of Young's modulus obtained at room temperature for the non-hydrided prior-β_{Zr} material is consistent with those measured by Stern et al. [14] by using a resonance method (dynamic Young's modulus) on prior-β_{Zr} samples elaborated from a Zircaloy-4 sheet, which are by the way close to those reported in [60] and [61] for the as-received material (no heat-treatment in the β_{Zr} temperature domain before testing). The results show that the Young's modulus of the (prior-) β_{Zr} phase, hydrogenated or not, decreases with increasing the temperature between 20 and 700°C. The evolution as a function of temperature is not very different from those predicted by the correlations given in [60] and [61] for the as-received material.

Taking into account the uncertainty on measurements and the significant scattering of results, no significant effect of hydrogen up to about 3000 wt.ppm is evidenced whatever the temperature. Yamanaka et al. [70] observed that the Young's modulus between 20 and 500°C of pure α_{Zr} charged in hydrogen up to about 250 wt.ppm decreases with increasing hydrogen content when hydrogen is in solid solution and slightly increases when hydrogen is partially precipitated under the form of hydrides. The oxygen content of the hydrogenated samples is a few hundreds of wt.ppm higher than that of the as-received material (due to oxygen absorption during hydrogen charging). However, oxygen does not have a significant effect on elastic properties within this concentration range [7][14]. Oxide and $\alpha_{Zr}(O)$ layers grow during the heat-treatment in air up to the β_{Zr} temperature domain, applied before mechanical testing. These phases, which are probably not already cracked at the beginning of the tensile test, have Young's moduli higher than the (prior-) β_{Zr} phase [7][14][60]. However, these layers are relatively thin (about 5-10 μm so that the cumulated thickness of these layers is around 5% of the cladding wall-thickness) and their contribution to the measured Young's modulus is expected to be within experimental uncertainty.

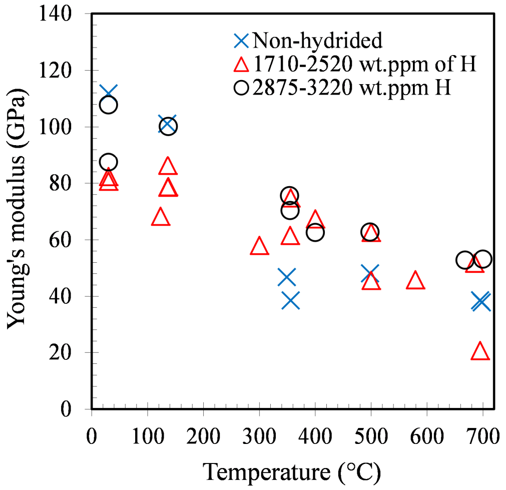

FIG. 14—*Evolution as a function of temperature of the Young's modulus (accuracy of about ±10 GPa) of model (prior-)* β_{Zr} *materials, non-hydrided or containing between 1710 and 3220 wt.ppm of hydrogen (and at least 0.2 wt.% of oxygen).*

Fracture—The non-hydrided model (prior-) β_{Zr} material is ductile whatever the temperature upon cooling between 20 and 700°C (Fig. 15 and Fig. 16), in accordance with Sawatzky [8] or Stern et al.' [14] results for example. Plastic elongation and cross-sectional reduction of area at fracture reach several percents at room temperature and increase with increasing temperature. Reduction of area at failure is nearly 100% at 700°C. The values of plastic elongation at failure are consistent with those obtained by Stern et al. [14] from tensile tests performed between 20 and 260°C on model non-hydrided prior-β_{Zr} sheet specimens with a gauge part of the same size as the cladding specimens tested in the present study. As shown in Fig. 15 and Fig. 16, the model (prior-) β_{Zr} material is embrittled by hydrogen contents of 2000-3000 wt.ppm for a given temperature below 500°C. The material becomes macroscopically brittle at 135°C and below for an average hydrogen content of about 2000 wt.ppm and at 350-400°C for a content of about 3000 wt.ppm. At 20 and 135°C, maximum stress at failure of the hydrided material, brittle macroscopically, decreases with increasing the hydrogen content within the 2000-3000 wt.ppm range (Fig. 17(b)). Stress at failure is about 300 MPa in the more brittle case tested (sample with 3210 wt.ppm of hydrogen tested at room temperature).

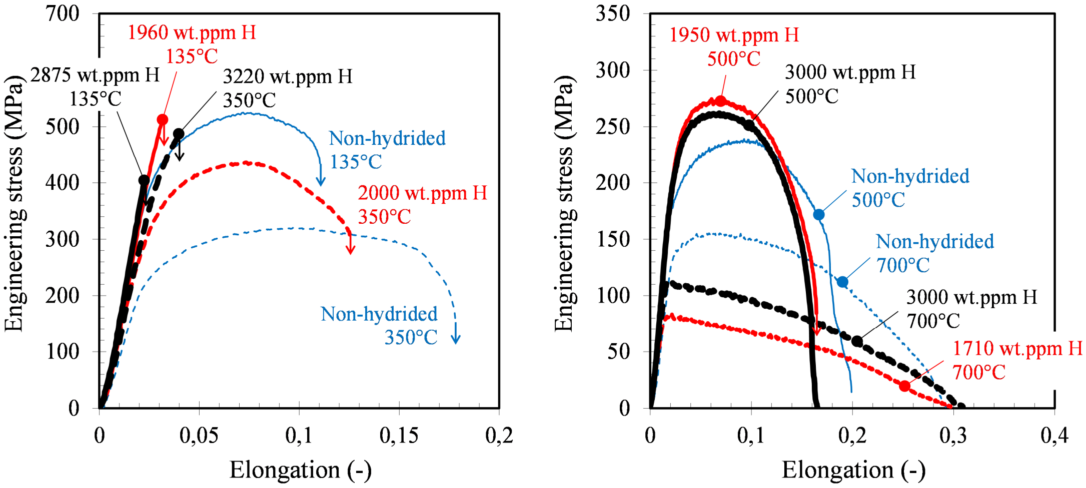

(a) (b)

FIG. 15—*Examples of engineering stress-strain (deduced from cross-head displacement) curves obtained (a) at 135 and 350°C and (b) at 500 and 700°C for model (prior-)* β_{Zr} *materials, non-hydrided or containing between 1710 and 3220 wt.ppm of hydrogen (and at least 0.2 wt.% of oxygen).*

The effect of hydrogen on macroscopic ductility diminishes when the temperature increases (Fig. 16). It becomes negligible beyond 500°C. The cross-sectional reduction at failure is nearly 100% at 580 and 700°C even for the highest hydrogen contents investigated. Thus, according to these results, the macroscopic failure mode of the model (prior-) β_{Zr} material undergoes a ductile-to-brittle transition as the hydrogen content is increased and the temperature is decreased. This is illustrated in Fig. 18 where the material is considered to be brittle, nearly brittle and ductile when the plastic strain at failure is lower than 0.005, between 0.005 and 0.01 and higher than 0.01, respectively. This figure also includes data from the literature (their characteristics are given in Table 4). Results reported by Stuckert et al. [62] and Pshenichnikov et al. [38] suggest that the prior-β_{Zr} material is ductile at room temperature even for hydrogen contents as high as 3000 wt.ppm. This difference compared to the present results or to those published by Brachet et al. [3], which showed that the prior-β_{Zr} material with about 600 wt.ppm of hydrogen is almost brittle at room temperature, may be at least partly due to a difference in the cooling scenario: cooling down from 800-927°C in air at room temperature with an initial rate of about 5°C/s for Stuckert et al. [62] and Pshenichnikov et al. [38], cooling rate varying between about 5 and 1°C/s from 1200°C down to 500°C and slower below in the present case, direct water quenching from 1000°C for Brachet et al. [3]. Indeed, it has been shown for Zircaloy-4 pre-hydrided at about 600 wt.ppm and oxidized at 1200°C that the post-quench hardening and macroscopic ductility at room temperature strongly depend on the partitioning of oxygen and hydrogen that occurs upon cooling during the β_{Zr} to α_{Zr} allotropic phase transformation and are directly related to the cooling rate during this transformation [64]. Typically, an increase in cooling rate during the β_{Zr} to α_{Zr} phase transformation induces an increase in the resultant prior-β_{Zr} hardening and an associated decrease in macroscopic ductility. Furthermore, the differences between the present results and those reported in [38] and [62] may be attributed to the slightly higher oxygen content of the materials tested here due to oxygen absorption and diffusion during hydrogen-charging and heat-treatment in the β_{Zr} temperature domain before tensile testing.

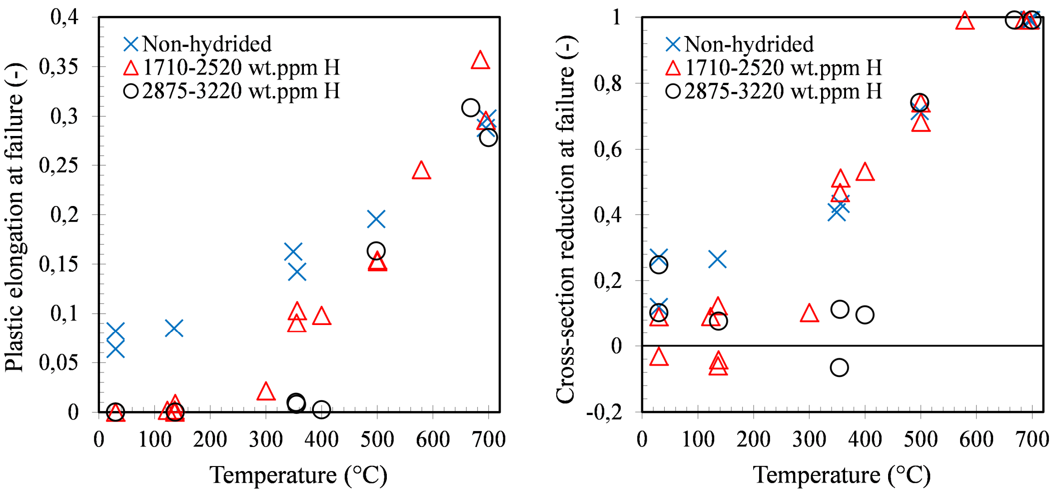

(a) (b)

FIG. 16—*Evolution as a function of temperature of (a) the plastic elongation at failure and (b) the reduction of area at fracture (accuracy of about ±0.08) obtained for model (prior-)* β_{Zr} *materials, non-hydrided or containing between 1710 and 3220 wt.ppm of hydrogen (and at least 0.2 wt.% of oxygen).*

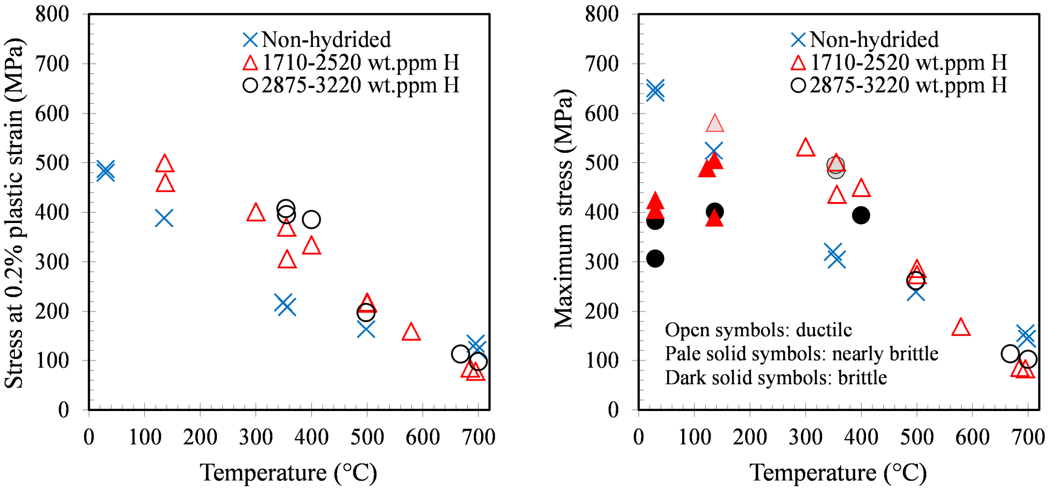

(a) (b)

FIG. 17—*Evolution as a function of temperature of (a) the yield stress at 0.2% plastic strain and (b) the ultimate (maximum) stress obtained for model (prior-)* β_{Zr} *materials, non-hydrided or containing between 1710 and 3220 wt.ppm of hydrogen (and at least 0.2 wt.% of oxygen).*

TABLE 4—*Data from the literature on the mechanical behavior of Zircaloy-4, pre-hydrided or not, heat-treated in the* β_{Zr} *temperature domain, illustrated in Fig. 18.*

Reference	Material	Cooling from the β_{Zr} temperature domain	Mechanical testing after cooling
Brachet et al. [3]	Cladding tube, pre-hydrided up to about	Water quenching from 1000°C	Impact, ring compression and 3 point bending tests

	600 wt.ppm or not		at 20 and 135°C
Stern et al. [14]	Sheet, non-hydrided	Water quenching from 1200 or 1300°C	Tensile tests between -100 and 260°C
Cabrera [63]	Sheet, pre-hydrided up to about 600 wt.ppm or not	Water quenching from 1200 or 1300°C	Tensile tests at 20 and 135°C
Stuckert et al. [62]	Cladding tube, pre-hydrided up to 2800 wt.ppm	Cooling down from 800 or 900°C in air at room temperature with an initial rate of about 5°C/s	Ring compression and axial tensile tests at 20°C
Pshenichnikov et al. [38]	Cladding tube, pre-hydrided up to 10000 wt.ppm	Cooling down from 827 or 927°C in air at room temperature with an initial rate of about 5°C/s	Axial tensile tests 20°C

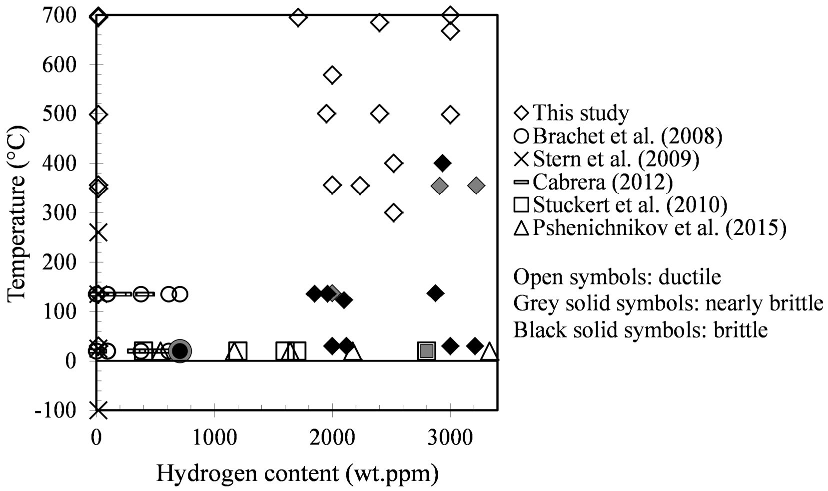

FIG. 18—*Ductile or brittle fracture modes of the (prior-)* β_{Zr} *phase as a function of temperature and mean hydrogen content; data from this study and from Brachet et al. [3], Stern et al. [14], Cabrera [63], Stuckert et al. [62] and Pshenichnikov et al. [38] (features given in Table 3).*

Fracture surface of brittle samples (hydrogen-charged materials tested at low temperature) is macroscopically perpendicular to the principal loading direction. After testing at 20 and 135°C, topography of the fracture surface of the material with a mean hydrogen content of about 2000 wt.ppm appears to be a little bit rougher than in the case of the material containing about 3000 wt.ppm of hydrogen. This slight difference may be due to a higher volume fraction of proeutectoid α_{Zr} phase in the case of the lowest hydrogen content, as already discussed before in the paragraph dealing with the microstructure of the model materials right after hydrogen charging. Fracture surface of ductile specimens exhibits a rough topography and is macroscopically slanted in most cases. In the most ductile cases, above 500°C typically, macroscale fracture occurs mainly by through-thickness necking. Multiple cracking of the oxide layers (cracks perpendicular to the tensile direction) was observed at the surface of the samples that failed after significant plastic deformation (crack density is higher near the sample fracture surface, where axial strains and stresses were higher due to necking). No macroscopic cracks were observed at the oxide surface on the brittle samples that failed in the elastic regime.

Observation by SEM of the fracture surfaces shows that the thin oxide and α_{Zr}(O) layers at samples surfaces fail in a brittle manner at least for temperatures up to 500°C (the fracture mode at 700°C was not clearly identified), in accordance with the results presented in the previous section of this paper dedicated to the behavior α_{Zr}(O) phase. As illustrated in Fig. 19(a), SEM examination reveals the presence of dimples on the fracture surface of the non-hydrided model (prior-) β_{Zr} material for all the tested temperatures between 20 and 700°C (the non-hydrided material is fully transformed into the α_{Zr} (prior-β_{Zr}) phase at these temperatures).

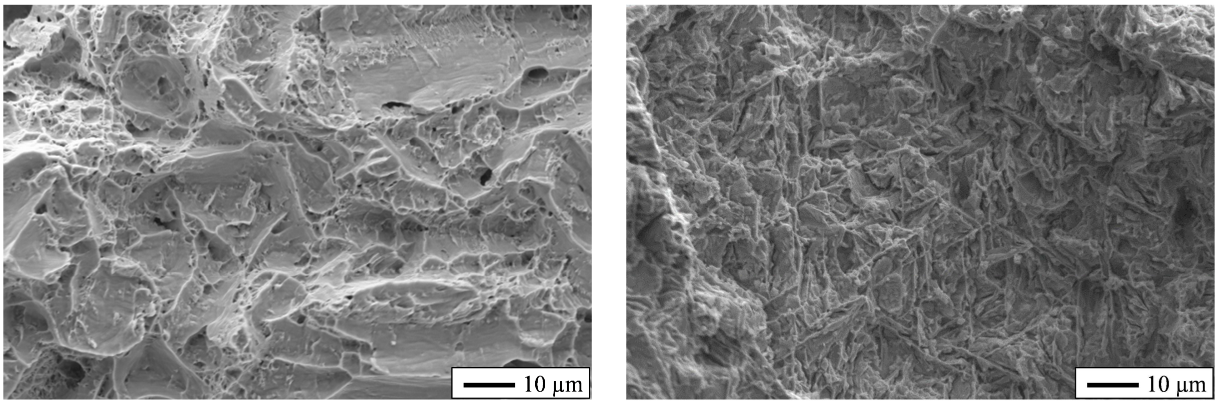

(a) non-hydrided, test at 135°C, macroscopically ductile

(b) 2000 wt.ppm of hydrogen, test at 135°C, macroscopically nearly brittle

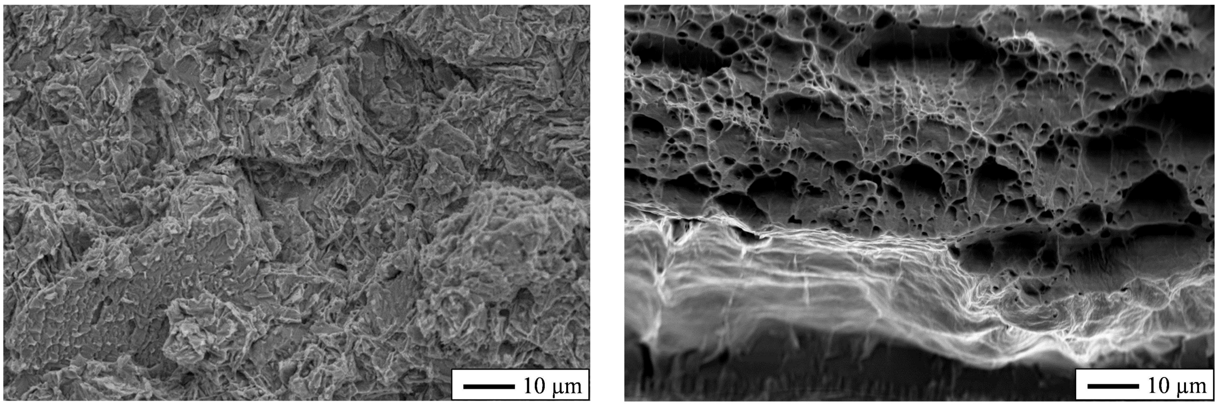

(c) 2875 wt.ppm of hydrogen, test at 135°C, macroscopically brittle

(d) 3000 wt.ppm of hydrogen, test at 500°C, macroscopically ductile

FIG. 19—*SEM micrographs of the fracture surfaces of model (prior-) β_{Zr} samples, non-hydrided or containing 2000 to 3000 wt.ppm of hydrogen (and at least 0.2 wt.% of oxygen), fractured at 135 and 500°C.*

At 500°C and below, the material highly charged in hydrogen is constituted of a mixture of oxygen enriched and hydrogen depleted zones (proeutectoid α_{Zr} phase) and hydrogen enriched zones (α_{Zr} phase appeared below the eutectoid temperature). Features of brittle fracture are observed at the microscale on the fracture surface of the hydrogen-charged materials that show a brittle behavior macroscopically, but zones of ductile fracture are also detected between the brittle fracture zones (Fig. 19(b) and (c)). The lower the fraction of these ductile zones, the more the material is brittle macroscopically. During cooling and β_{Zr} to α_{Zr} phase transformation, a partitioning of chemical elements and in particular of hydrogen and oxygen occurs between β_{Zr} and α_{Zr} (prior-β_{Zr}) phases, resulting in chemical fluctuations at the microscale: typically, the first regions to transform during cooling into α_{Zr} phase are depleted in hydrogen and enriched in oxygen and the last transformed zones are enriched in hydrogen and depleted in oxygen. This partitioning depends on the mean hydrogen and oxygen contents and the cooling scenario [64][67]. As a consequence, as already suggested in [14] for the oxygen-charged prior-β_{Zr} phase and in [66] for the hydrogen-charged prior-β_{Zr} phase, it seems that the fracture of the model prior-β_{Zr} phase elaborated from Zircaloy-4 charged in hydrogen up to more than 2000 wt.ppm in average (and slightly enriched in oxygen) initiates in a brittle manner in regions enriched in hydrogen (as a result of chemical elements partitioning during cooling) and that the final fracture mainly occurs by ductile tearing of the surrounding regions depleted in hydrogen. Even if the underlying mechanisms are not the same, this failure mode mixing brittle and ductile fracture at the microscale has similarities in appearance to the fluted fracture that may occur for example in transgranular stress-corrosion cracking conditions [68]. These observations show that the ductile-to-brittle transition of the hydrogen-enriched (prior-) β_{Zr} phase material is not as marked at the microscale as at the macroscale, as also observed by Stern et al. [14] for oxygen-charged prior-β_{Zr} phase.

No “macroscopic” hydrides could be clearly detected by optical or scanning electron microscopy after testing. However, recent results show that hydrogen precipitates in the form of fine intergranular δ and γ zirconium hydrides during cooling from the β_{Zr} temperature domain and suggest that a small fraction of hydrogen should remain in solid solution within the α_{Zr} matrix [38][65][66]. Deeper analyses should be performed to determine the exact location, morphology and orientation of hydrides. The mechanisms responsible for the observed hydrogen-induced embrittlement are still not clearly identified and require further investigation. An overview on potential hydrogen-induced embrittlement mechanisms (hydride fracture, hydrogen-enhanced decohesion, hydrogen-enhanced localized plasticity, adsorption-induced dislocation emission and hydrogen-vacancy interactions) was made in [71]. By taking into account the work of Yamanaka et al. [69][70], Pshenichnikov et al. [66] have suggested that hydrogen-induced embrittlement in highly hydrogen-enriched material is due to a decohesion mechanism, related to a decrease in the presence of hydrogen atoms of the strength of the bonds between Zr atoms.

After testing at 500°C, no significant difference of appearance is detected between the fracture surfaces of the non-hydrided material and the materials with about 2000 and 3000 wt.ppm of hydrogen, on which dimples are observed (Fig. 19(d)). For both non-hydrided and hydrogen-charged specimens tested at 700°C (and at 580°C for a mean hydrogen content of about 2000 wt.ppm), a nearly complete reduction in thickness is observed at failure location. In other words, hydrogen up to contents of about 3000 wt.ppm has no visible effect on the fracture mechanisms beyond 500°C. According to recent results of thermodynamic calculations and *in-situ* neutron diffraction experiments [65], at 500°C, hydrogen, for a content of thousands of wt.ppm, is still expected to be partially precipitated in the form of δ hydrides. The absence of significant embrittlement effect of hydrogen at this temperature may be due to a lower fraction of precipitated hydrogen, a higher ductility of hydrides and/or a reduction of the potential weakening effect of hydrogen on the interatomic bonds (hydrogen-enhanced decohesion). The material containing 2000-3000 wt. ppm of hydrogen in average is expected to be constituted of β_{Zr} phase (with potentially a small fraction of proeutectoid α_{Zr} phase) at 700°C and of a mixture of proeutectoid α_{Zr} phase (depleted in hydrogen and enriched in oxygen) and β_{Zr} phase (enriched in hydrogen and depleted in oxygen) at 580°C (the highest the hydrogen content, the lowest the fraction of proeutectoid α_{Zr} phase). Beyond the eutectoid temperature (around 550°C), hydrogen is fully dissolved in the Zr lattice and therefore it is not surprising that hydrogen, only present in solute, has no significant embrittlement effect at 580 and 700°C.

Plasticity—As shown in Fig. 15 and Fig. 17, flow stress of the non-hydrided prior-β_{Zr} phase decreases with increasing the temperature between 20 and 700°C. The limited amount of oxygen that potentially diffused into the material during the heat-treatment at HT before tensile testing has probably a slight strengthening effect [60]. Furthermore, it cannot be excluded that the thin oxide and α_{Zr}(O) layers at samples surfaces slightly contribute to the samples global mechanical response at the beginning of plastic regime. The values of ultimate stress are relatively close to those obtained by Sawatzky [8] from hoop tensile tests performed at a strain rate of about $3 \cdot 10^{-3}$ s^{-1} on non-hydrided Zircaloy-2 cladding specimens heat-treated in the β_{Zr} temperature domain and cooled at 20°C/s down to 850°C and then quicker down to room temperature. The values of ultimate stress obtained at 20 and 135°C are significantly lower than those reported by Stern et al. [14] for non-hydrided prior-β_{Zr} samples elaborated from a Zircaloy-4 sheet tested under tension with a strain rate of about $5 \cdot 10^{-4}$ s^{-1}. This last strain rate is 200 times slower than the one applied during the tests of the present study and cannot explain the differences in ultimate stresses (the flow stress is expected to decrease with decreasing the strain rate, as a result of viscoplasticity). These differences in ultimate stresses could be explained by the faster cooling rate applied in [14] in comparison to the present study after the incursion in the β_{Zr} temperature domain, resulting in a finer microstructure (and perhaps a more pronounced “martensitic-type” microstructure) with a higher mechanical resistance.

Comparison of the results obtained for the non-hydrided prior-β_{Zr} phase material and the material containing between about 1700 and 3200 wt.ppm of hydrogen reveals at temperatures of 500°C and below an increase of the flow stress with increasing the hydrogen content when the material is macroscopically ductile (*i.e.* for temperatures higher than 135°C and 350-400°C for mean hydrogen contents of about 2000 wt.ppm and 3000 wt.ppm, respectively) (Fig. 17). For example, at 350°C, the ultimate stress increases from about 320 MPa for the non-hydrided material to about 450 MPa for the material containing about 2000 wt.ppm of hydrogen, which corresponds to a relative increase of about 20%. This strengthening effect diminishes when temperature increases. Due to oxygen absorption during hydrogen-charging, the oxygen content is higher of about 0.07 wt.% in the hydrided samples than in the non-hydrided material. According to the model proposed in [60], an increase of 0.07 wt.% of the oxygen content induces, for a given plastic strain, a relative increase of about 9% of the flow stress for temperatures between 20 and 700°C. Therefore, it can be considered that hydrogen has definitely a strengthening effect at 400°C and below. This is in agreement with the results of Pshenichnikov et al. [38] that show an increase in strength (and a decrease in ductility) of the prior-β_{Zr} phase (elaborated from Zircaloy-4) at room temperature when increasing the hydrogen content up to several hundreds of wt.ppm. Hydrogen also induces hardening of the prior-β_{Zr} phase at room temperature [3][33][38]. The increase in mechanical resistance of the prior-β_{Zr}

phase in the presence of high hydrogen contents at 500°C and below can be related to the particular microstructure of the material. The material can be seen as a complex micro-composite material made of a mixture of proeutectoid α_{Zr} (prior-β_{Zr}) phase, enriched in oxygen and depleted in hydrogen, and prior-β_{Zr} phase transformed below the eutectoid temperature, slightly depleted in oxygen but containing a very large amount of hydrogen, expected to be, at least partially, precipitated under the form of hardener nano-hydrides.

At 700°C, the material containing 1700 to 3000 wt.ppm of hydrogen has a lower flow stress than the non-hydrided material. At this temperature, all hydrogen is in solid solution in the zirconium matrix, expected to be mainly in the β_{Zr} phase (with potentially a little fraction of proeutectoid α_{Zr} phase), whereas the non-hydrided material is in the α_{Zr} (prior-β_{Zr}) phase. This lower flow stress at 700°C in the presence of high hydrogen content is likely due to a high volume fraction of β_{Zr} phase, which is known to have a lower mechanical resistance at HT than the α_{Zr} (prior-β_{Zr}) phase (and potentially, to a lesser extent, a decrease of the Zr-Zr bond order caused by solute hydrogen [70], a decrease of the dislocation pinning caused by interstitial atoms and/or the enhancement of dislocation mobility [44]). A softening effect of hydrogen in solid solution, as well as a strengthening effect of hydrides, was also reported for Zircaloy-4 in the α_{Zr} phase tested between 20 and 480°C [72][73].

No significant effect of temperature or hydrogen was evidenced on average values of ratios of axial to hoop plastic strain increments measured by digital image correlation within the specimen gauge part before necking. The measured ratios are not far from -0.5, characteristic of an isotropic plastic behavior. No significant effect of hydrogen for contents up to 1200 wt.ppm was observed either between 20 and 480°C for Zircaloy-4 in the α_{Zr} phase (without previous β_{Zr} heat-treatment) [73][74].

As illustrated in Fig. 20, uniform plastic strain of the non-hydrided prior-β_{Zr} phase does not evolve significantly between 20 and 135°C then increases with increasing the temperature between 135 and 500°C, in accordance with the results reported in [14] for non-hydrided prior-β_{Zr} specimens (elaborated from a Zircaloy-4 sheet) with dimensions equivalent to those of the specimens tested in the present study. This evolution of uniform elongation as a function of temperature is different from the decreasing tendency observed for as-received Zircaloy-4, in the α_{Zr} phase [61][73]. Uniform elongation of the non-hydrided prior-β_{Zr} phase is lower at 700°C than at 500°C. Hydrided samples with about 2000 wt.ppm and 3000 wt.ppm of hydrogen in average fail without necking at temperatures lower than 350°C and 500°C respectively (Fig. 15). When failure occurs after necking, uniform plastic strain is significantly lower for the material with about 2000-3000 wt.ppm of hydrogen than for the non-hydrided material (Fig. 20). At 700°C, necking of the highly hydrided materials (mainly or fully in the form of β_{Zr} phase at this temperature) occurs at the very beginning of macroscopic plasticity, for a plastic strain level lower than 0.01. In other words, plastic strain localization is enhanced in the presence of high hydrogen contents (when the material can withstand significant plastic strain before failure).

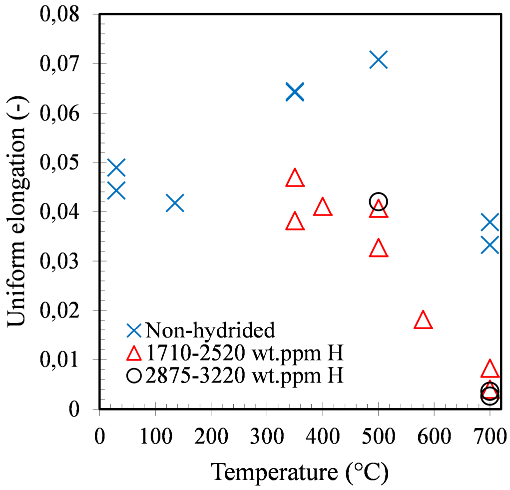

FIG. 20—*Evolution as a function of temperature of the uniform elongation (plastic strain at the maximum stress when failure occurs after necking) obtained for model (prior-)* β_{Zr} *materials, non-hydrided or containing between 1710 and 3220 wt.ppm of hydrogen (and at least 0.2 wt.% of oxygen).*

Partial conclusion

Model materials homogeneously enriched in hydrogen at various contents between 1700 and 3200 wt. ppm were elaborated from Zircaloy-4 cladding tubes to investigate the effects of high hydrogen contents on the mechanical behavior of the (prior-) β_{Zr} phase. These materials have been submitted to axial tensile tests in air at various temperatures between 20 and 700°C, upon cooling from the β_{Zr} temperature domain. Mechanical strength and ductility of the model (prior-) β_{Zr} phase material are shown to be affected by high hydrogen contents in ways that strongly depend on temperature. The results have been related to the metallurgical evolutions that occur at HT and upon cooling.

Conclusions

Oxygen and hydrogen are known to be the main parameters responsible for embrittlement of zirconium alloys.

Model materials homogeneously enriched in oxygen at various contents between 2 and 5.8 wt.% were elaborated from M5® cladding tubes to investigate the effects of high oxygen contents on the mechanical behavior of the $\alpha_{Zr}(O)$ phase at HT. Results of axial tensile creep tests performed under vacuum between 800 and 1100°C show that the creep resistance of the oxygen-enriched $\alpha_{Zr}(O)$ material increases with increasing oxygen content. It is significantly higher than the creep resistance of the as-received material without additional oxygen. Two creep regimes are observed: a power-law regime for stresses higher than 15 MPa and a nearly linear regime for lower stresses. Model $\alpha_{Zr}(O)$ materials are ductile between 800 and 1100°C for oxygen contents between 2 and 3.2 wt.% but become brittle, even at 1100°C, for oxygen contents higher than 4 wt.%. Deformation and failure mechanisms, and influence of microstructural features of the model oxygen-enriched $\alpha_{Zr}(O)$ materials (residual β_{Zr} phase, grain morphology, …), have been analyzed. However, further investigation is needed to identify the mechanisms that drive the linear creep regime observed at low stresses. A model is proposed to describe the oxygen content dependent viscoplastic behavior of the $\alpha_{Zr}(O)$ phase. Finite element analysis performed by using this model for the α_{Zr}(O) phase layer highlights the strengthening effect of this layer on the creep behavior of cladding tubes oxidized at HT submitted to an internal pressure at HT. These data could also be of interest regarding the behavior of the oxidized cladding, which depends on the properties of each phase/layer, during the oxidation at HT and the subsequent cooling and quenching at the end of a LOCA-like transient.

The mechanical behavior of the (prior-) β_{Zr} phase highly enriched in hydrogen was investigated through axial tensile tests performed in air at various temperatures between 20 and 700°C, upon cooling from the β_{Zr} temperature domain, on model (prior-) β_{Zr} phase materials elaborated from Zircaloy-4 cladding tubes, homogeneously enriched in hydrogen at various contents between about 1700 and 3200 wt. ppm. The Young's modulus of the (prior-) β_{Zr} phase decreases with increasing temperature and is not much affected by hydrogen. Ductility of the model (prior-) β_{Zr} phase material increases with increasing temperature. The material is embrittled by hydrogen for temperatures below 500°C. It becomes macroscopically brittle at 135°C and below for an average hydrogen content of about 2000 wt.ppm and at 350-400°C for about 3000 wt.ppm of hydrogen. The effect of hydrogen on macroscopic ductility diminishes when temperature increases and becomes negligible beyond 500°C. When the behavior is macroscopically ductile, the flow stress of the (prior-) β_{Zr} phase containing between 1700 and 3200 wt.ppm of hydrogen is higher than the one of the non-hydrided material at 500°C and below, and lower at 700°C. Plastic isotropy is not substantially modified by hydrogen. Plastic strain localization occurs sooner in the highly hydrided material, when significant plastic strain occurs before failure. The results are related to the complex (temperature and mean hydrogen content dependent) microstructure of the highly hydrided (prior-) β_{Zr} phase material, resulting from segregation of hydrogen and other chemical elements, phase transformations beyond and below the eutectoid temperatures and hydride precipitation. These data could be useful to assess the mechanical response, during and after quenching at the end of a LOCA transient, of the (prior-) β_{Zr} phase in the regions of a ballooned/burst cladding that have experienced a significant secondary hydriding during HT steam oxidization. However, further work has to be done to determine the underlying mechanisms responsible for the effects of high hydrogen contents on the mechanical behavior of the (prior-) β_{Zr} phase.

The results presented in this paper were obtained on model oxygen-enriched α_{Zr}(O) phase and hydrogen-enriched (prior-) β_{Zr} phase materials respectively elaborated from M5® and Zircaloy-4 cladding tubes. The conclusions are not necessarily directly applicable to other alloys.

Acknowledgments

The authors would like to thank D. Hamon, V. Lezaud, E. Rouesne, S. Urvoy, C. Toffolon-Masclet, P. Bonnaillie, M.H. Mathon, C. Raepsaet and G. Bayon from CEA, and J. Heurtel, A. Laurent, J.D. Bartout, A. Meddour, A. Koster and J.C. Teissedre from the Centre des Matériaux (Mines ParisTech) for their contribution to this work. The authors thank AREVA and EDF for their financial contribution to this work. AREVA is also acknowledged for material supply.

References

[1] Sawatzky, A., Ledoux, G.A. and Jones, S., "Oxidation of zirconium during a high-temperature transient," *Zirconium in the Nuclear Industry, ASTM STP 633*, A. L. Lowe, Jr. and G. W. Parry, Eds., American Society for Testing and Materials, 1977, pp. 134-149.

[2] Chung, H.M., Garde, A.M. and Kassner, T.F., "Development of an Oxygen Embrittlement Criterion for Zircaloy Cladding Applicable to Loss-of-Coolant Accident Conditions in Light-Water Reactors," *Zirconium in the Nuclear Industry (Fourth Conference), ASTM STP 681*, American Society for Testing and Materials, 1979, pp. 600-627.

[3] Brachet, J.C., Vandenberghe-Maillot, V., Portier, L., Gilbon, D., Lesbros, A., Waeckel, N. and Mardon, J.P., "Hydrogen Content, Preoxidation, and Cooling Scenario Effects on Post-Quench Microstructure and Mechanical Properties of Zircaloy-4 and M5® Alloys in LOCA Conditions," *Journal of ASTM International*, Vol. 5, 2008.

[4] Woo, O.T. and Tangri, K., "Transformation characteristics of rapidly heated and quenched Zircaloy-4-oxygen alloys," *Journal of Nuclear Materials*, Vol. 79, 1979, pp. 83-94.

[5] Leistikow, S., Schanz, G., "Oxidation Kinetics and Related Phenomena of Zircaloy-4 Fuel Cladding Exposed to High Temperature Steam and Hydrogen-Steam Mixtures under PWR Accident Conditions," *Nuclear Engineering and Design*, Vol. 103, 1987, pp. 65-84.

[6] Erbarcher, F.J., Neitzel, H.J., Rosinger, H.E., Schmidt, H. and Wiehr, K., "Burst Criterion of Zircaloy Fuel Claddings in a Loss-of-Coolant Accident," *Zirconium in the Nuclear Industry: Fifth Conference, ASTM STP 754*, D.G. Frankin, Ed., American Society for Testing and Materials, 1982, pp. 271-283.

[7] Bunnell, L.R. and Bates, J.L., Mellinger, G.B., "Some high-temperature properties of Zircaloy-oxygen alloys," *Journal of Nuclear Materials*, Vol. 116, 1983, pp. 219-232.

[8] Sawatzky, A., "A proposed criterion for the oxygen embrittlement of Zircaloy-4 fuel cladding," *Zirconium in the Nuclear Industry (Fourth Conference), ASTM STP 681*, American Society for Testing and Materials, 1979, pp. 479-496.

[9] Rizkalla, A.S., Holt, R.A., Jonas, J.J., "Effect of oxygen on the deformation of Zircaloy-2 at elevated temperatures," *Zirconium in the Nuclear Industry (Fourth Conference), ASTM STP 681*, American Society for Testing and Materials, 1979, pp. 497-513.

[10] Burton, B., Donaldson, A.T. and Reynolds, G.L., "Interaction of Oxidation and Creep in Zircaloy-2," *Zirconium in the Nuclear Industry (Fourth Conference), ASTM STP 681*, American Society for Testing and Materials, 1979, pp. 561-585.

[11] Choubey, R., Jonas, J.J., Holt, R.A. and Ells, C.E., "Flow stress of oxygen-enriched Zircaloy-2 between 1023 and 1873 K," *Zirconium in the Nuclear Industry: Fifth Conference, ASTM STP 754*, D.G. Frankin, Ed., American Society for Testing and Materials, 1982, pp. 350-369.

[12] Chow, C.K., Rosinger, H.E. and Bera, P.C., "Creep behaviour of oxidized Zircaloy-4 fuel sheathing," *Proceedings of the Materials in Nuclear Energy Conference*, Huntsville, Canada, September 29-October 2, 1982, pp. 112-116.

[13] Tseng, D. and Tangri, K., "Deformation Behavior of Duplex Zircaloy-4-Oxygen Alloys," *Metallurgical Transactions A*, Vol. 13A, 1982, pp. 1077-1082.

[14] Stern, A., Brachet, J.C., Maillot, V., Hamon, D., Barcelo, F., Poissonnet, S. and Pineau, A., Mardon, J.P., Lesbros, A., "Investigations of the Microstructure and Mechanical Properties of Prior-β Structure as a Function of the Oxygen Content in Two Zirconium Alloys," *Journal of ASTM International*, Vol. 5, No. 4, 2009, JAI101119, pp. 71-118.

[15] Bossis, P., Pêcheur, D., Hanifi, K., Thomazet, J. and Blat, M., "Comparison of the High Burn-up Corrosion on M5 and Low Tin Zircaloy-4," *Journal of ASTM International*, Vol. 3, No. 1, 2008, pp. 494-525.

[16] Mardon, J.P., Garner, G. and Hoffmann, P.B., “M5® a Breakthrough in Zr Alloy,” *Proceedings of the International Topical Meeting on Light Water Reactor Fuel Performance*, Orlando, USA, September 26-29, 2010, pp. 577-586.

[17] Park, K., Kim, K.P., Yoo, T.G. and Kim, K.T., “Pressure effects on high temperature steam oxidation of Zircaloy-4,” *Metals and Materials International*, Vol. 7, 2001, pp. 367-373.

[18] Le Saux, M., Vandenberghe, V., Crébier, P., Brachet, J.C., Gilbon, D., Mardon, J.P. and Sebbari, B., “Influence of steam pressure on the high temperature oxidation and post-cooling mechanical properties of Zircaloy-4 and M5™ cladding (LOCA conditions),” *Zirconium in the Nuclear Industry: 17th International Symposium, STP 1543*, ASTM International, West Conshohocken, PA, 2014, pp. 1002-1053.

[19] Leistikow, S. and Schanz, G., “Oxidation Kinetics and Related Phenomena of Zircaloy-4 Fuel Cladding Exposed to High Temperature Steam and Hydrogen-Steam Mixtures under PWR Accident Conditions,” *Nuclear Engineering and Design*, Vol. 103, 1987, pp. 65-84.

[20] Portier, L., Bredel, T., Brachet, J. C., Maillot, V., Mardon, J. P., and Lesbros, A., “Influence of Long Service Exposures on the Thermal-Mechanical Behaviour of Zy-4 and M5 Alloys in LOCA Conditions,” *Journal of ASTM International*, Vol. 2, No. 2, 2005, JAI12468.

[21] Baek, J.H. and Jeong, Y.H., “Breakaway Phenomenon of Zr-Based Alloys During a High-Temperature Oxidation,” Journal of Nuclear Materials, Vol. 372, 2008, pp. 152-159.

[22] Vandenberghe, V., Brachet, J.C., Le Saux, M., Gilbon, D., Mardon, J.P. and Sebbari, B., “Sensitivity to chemical composition variations and heating/oxidation mode of the breakaway oxidation in M5® cladding steam oxidized at 1000°C (LOCA conditions),” *Proceedings of TopFuel 2012*, Manchester, UK, September 2-6, 2012.

[23] Uetsuka, H., Furuta, T. and Kawasaki, S., “Failure-Bearing Capability of Oxidized Zircaloy-4 Cladding under Simulated Loss-of-Coolant Condition,” *Journal of Nuclear Science and Technology*, Vol., No. 11, 1983, pp. 941-950.

[24] Billone, M., Yan, Y., Burtseva, T. and Daum, R., “Cladding Embrittlement during Postulated Loss-of-Coolant Accidents,” NUREG/CR-6967, 2008.

[25] Nagase, F. and Fuketa, T., “Behavior of Pre-hydrided Zircaloy Cladding under Simulated LOCA Conditions,” *Journal of Nuclear Science and Technology*, Vol. 42, No. 2, 2005, pp. 209-218.

[26] Stuckert, J., Große, M., Rössger, C., Klimenkov, M., Steinbrück, M. and Walter, M., “QUENCH-LOCA program at KIT on secondary hydriding and results of the commissioning bundle test QUENCH-L0,” *Nuclear Engineering and Design*, Vol. 225, 2013, pp. 185-201.

[27] Furuta, T. and Kawasaki, S., “Reaction behavior of zircaloy-4 in steam-hydrogen mixtures at high temperature,” *Journal of Nuclear Materials*, Vol. 105, No. 2-3, 1982, pp. 119-131.

[28] Veshchunov, M.S. and Shestak, V.E., “Modeling of Zr alloy burst cladding internal oxidation and secondary hydriding under LOCA conditions,” *Journal of Nuclear Materials*, Vol. 461, 2015, pp. 129-142.

[29] Große, M., Stuckert, J., Steinbrück, M. and Kaestner, A., “Secondary hydriding during LOCA – Results from the QUENCH-L0 test,” *Journal of Nuclear Materials*, Vol. 420, No. 1-3, 2012, pp. 575-582.

[30] Raepsaet, C., Bossis, P., Hamon, D., Béchade, J.L. and Brachet, J.C., “Quantification and local distribution of hydrogen within Zircaloy-4 PWR nuclear fuel cladding tubes at the nuclear microprobe of the Pierre Süe Laboratory from µ-ERDA,” *Nuclear Instruments and Methods in Physics Research B*, Vol. 266, 2008, pp. 2424-2428.

[31] Brachet, J.C., Hamon, D. and Raepsaet, C., “Capability of EPMA et µ-ERDA to quantify the micro-chemical partitioning within nuclear fuel cladding materials after a LOCA transient,” *presented at Workshop on LOCA*, Lyon, France, May 29-30, 2012.

[32] Nagase, F. and Fuketa, T., “Effect of Pre-Hydriding on Thermal Shock Resistance of Zircaloy-4 Cladding under Simulated Loss-of-Coolant Accident Conditions,” *Journal of Nuclear Science and Technology*, Vol. 41, No. 7, 2004, pp. 723-730.

[33] Desquines, J., Drouan, D., Guilbert, S. and Lacote, P., “Embrittlement of pre-hydrided Zircaloy-4 by steam oxidation under simulated LOCA transients,” *Journal of Nuclear Materials*, Vol. 469, 2016, pp. 20-31.

[34] Yueh, H.K., Comstock, R.J., B., D., Le Saux, M., Lin, Y.P., Lutz, D., Park, D.J., Perez-Fero, E. and Yan, Y., “Loss of Coolant Accident Testing Round Robin,” *Proceedings of the LWR Fuel Performance Meeting / TopFuel 2013*, Charlotte, NC, USA, September 15-19, 2013.

[35] Le Saux, M., Brachet, J.C., Vandenberghe, V., Gilbon, D., Mardon, J.P. and Sebbari, B., “Influence of Pre-Transient Oxide on LOCA High Temperature Steam Oxidation and Post-Quench Mechanical Properties of Zircaloy-4 and M5™ cladding,” *Proceedings of the 2011 Water Reactor Fuel Performance Meeting*, Chengdu, China, September 11-14, 2011.

[36] Mazères, B., Desgranges, C., Toffolon-Masclet, C. and Monceau, D., “Contribution to Modeling of Hydrogen Effect on Oxygen Diffusion in Zy-4 Alloy During High Temperature Steam Oxidation,” *Oxidation of Metals*, Vol. 79, No. 1-2, 2013, pp. 121-133.

[37] Négyesi, M., Burda, J., Bláhová, O., Linhart, S. and Vrtílková, V., “The Influence of Hydrogen on Oxygen Distribution inside Zry-4 Fuel Cladding,” *Journal of Nuclear Materials*, Vol. 416, No. 3, 2011, pp. 288-292.

[38] Pshenichnikov, A., Stuckert, J. and Walter, M., “Microstructure and mechanical properties of Zircaloy-4 cladding hydrogenated at temperatures typical for loss-of-coolant accident (LOCA) conditions,” *Nuclear Engineering and Design*, Vol. 283, 2015, pp. 33-39.

[39] Chosson, R., Gourgues, A.F., Vandenberghe, V., Brachet, J.C. and Crépin, J., “Creep flow and fracture behavior of the oxygen-enriched alpha phase in zirconium alloys,” *Scripta Materialia*, accepted.

[40] Forgeron, T., Brachet, J.C., Barcelo, F., Castaing, A., Hivroz, J., Mardon, J.P. and Bernaudat, C., “Experiment and Modeling of Advanced Fuel Rod Cladding Behavior Under LOCA Conditions: Alpha-Beta Phase Transformation Kinetics and EDGAR Methodology,” *Proceedings of the 12th International Symposium on Zirconium in the Nuclear Industry, ASTM STP 1354*, ASTM International, West Conshohocken, PA, 2000, pp. 256-278.

[41] Kaddour, D., Frechinet, S., Gourgues, A.F., Brachet, J.C., Portier, L. and Pineau, A., “Experimental determination of creep properties of Zirconium alloys together with phase transformation,” *Scripta Materialia*, Vol. 51, 2004, pp. 515-519.

[42] Kaddour, D., Gourgues-Lorenzon, A.F., Brachet, J.C., Portier, P. and Pineau, A., “Microstructural influence on high temperature creep flow of Zr–1%NbO alloy in near- α, (α + β), and β temperature ranges in a high vacuum environment,” *Journal of Nuclear Materials*, Vol. 408, 2011, pp. 116-124.

[43] Dupin, N., Ansara, I., Servant, C., Toffolon, C., Lemaignan, C. and Brachet, J.C., “A Thermodynamic Database for Zirconium Alloys,” *Journal of Nuclear Materials*, Vol. 275, 1999, pp. 287-295.

[44] Toffolon, C., Guilbert, T. and Brachet, J.C., “Study of secondary intermetallic phase precipitation/dissolution in Zr alloys by high temperature–high sensitivity calorimetry,” Journal of Nuclear Materials, Vol. 372, 2008, pp. 367-378.

[45] Chosson, R., “Étude expérimentale et modélisation du comportement en fluage sous pression interne d’une gaine en alliage de zirconium oxydée en atmosphère vapeur,” PhD Thesis (in french), Mines ParisTech, France, 2014.

[46] Trego, G., “Comportement en fluage à haute température dans le domaine biphasé (α+β) du M5®,” PhD Thesis (in french), Mines ParisTech, France, 2011.

[47] Donaldson, A.T. and Evans, H.E., “Oxidation-induced creep in Zircaloy-2: II. Stress distribution in the oxygen-stabilised α-phase layer,” *Journal of Nuclear Materials*, Vol. 99, 1981, pp. 47-56.

[48] Nix, W.D., “The effects of grain shape on Nabarro-Herring and Coble creep processes,” Metals forum, Vol. 4, No. 1-2, 1981, pp. 38-43.

[49] Coble, R.L., “A Model for Boundary Diffusion Controlled Creep in Polycrystalline Materials,” *Journal of Applied Physics*, Vol. 34, No. 6, 1963, pp. 1679-1682.

[50] Herring, C., “Diffusional Viscosity of a Polycrystalline Solid,” *Journal of Applied Physics*, Vol. 21, 1950, pp. 437-445.

[51] Novotný, J., Fiala, J. and Cadek, J., “Harper-Dorn creep in alpha-zirconium,” *Acta Metallurgica*, Vol. 33, No. 5, 1985, pp. 905-911.

[52] Fiala, J. and Cadek, J., “Creep in zirconium at low stresses and temperatures from 748 to 973 K,” *Materials science and engineering*, Vol. 75, 1985, pp. 117-126.

[53] Prasad, N., Malakondaiah, G. and Rama Rao, P., “Low stress creep behaviour of zirconium,” *Transactions of the Indian Institute of Metals*, Vol. 42, 1989, pp. S165-S174.

[54] Kassner, M.E., Kumar, P. and Blum , W., “Harper-Dorn creep,” *International Journal of Plasticity*, Vol. 23, 2007, pp. 980-1000.

[55] Hood, G.M., “Point defect diffusion in alpha-Zr,” *Journal of Nuclear Materials*, Vol. 159, 1988, pp. 149-175.

[56] Garde, A., Chung, H.M. and Kassner, T.F., “Uniaxial Tensile Properties of Zircaloy Containing Oxygen: summary Report,” Report ANL-77-30, Argonne National Laboratory, 1977.

[57] Roddy, M.J., Cannon, W.R., Skandan, G. and Hahn, H., “Creep behavior of nanocrystalline monoclinic ZrO_2,” *Journal of the European Ceramic Society*, Vol. 22, 2002, pp. 2657-2662.

[58] Chokshi, A. H., “Diffusion, diffusion creep and grain growth characteristics of nanocrystalline and fine-grained monoclinic, tetragonal and cubic zirconia,” *Scripta Materialia*, Vol. 48, 2003, pp. 791-796.

[59] Yoshida, M., Shinoda, Y., Akatsu T. and Wakai, F., “Superplasticity-like deformation of nanocrystalline monoclinic zirconia at elevated temperatures,” *Journal of the American Ceramic Society*, Vol. 87, No. 6, 2004, pp. 1122-1125.

[60] Siefken, L.J., Coryell, E.W., Harvego, E.A. and Hohorst, J.K., “SCDAP/RELAP5/MOD 3.3 Code Manual: MATPRO - A Library of Materials Properties for Light-Water-Reactor Accident Analysis,” NUREG/CR-6150, 2001.

[61] Le Saux, M., Besson, J., Carassou, S., Poussard, C. and Averty, X., “A model to describe the anisotropic viscoplastic mechanical behavior of fresh and irradiated Zircaloy-4 fuel claddings under RIA loading conditions,” *Journal of Nuclear Materials*, Vol. 378, No. 1, 2008, pp. 60-69.

[62] Stuckert, J., Große, M. and Walter, M., “Mechanical properties of pre-hydrogenated (600 – 5000 wppm) cladding segments,” *Proceedings of the Quench Workshop 2010*, Karlsruhe, Germany, November 16-18, 2010.

[63] Cabrera Salcedo, A., “Modélisation du comportement mécanique "post-trempe", après oxydation à haute température des gaines de combustible des réacteurs à eau pressurisée,” PhD Thesis (in french), Mines ParisTech, France, 2012.

[64] Brachet, J.C., Hamon, D., Béchade, J.L., Forget, P., Toffolon-Masclet, C., Raepsaet, C., Mardon, J.P. and Sebbari, B., “Quantification of the chemical elements partitioning within pre-hydrided Zircaloy-4 after high temperature steam oxidation as a function of the final cooling scenario (LOCA conditions) and consequences on the (local) materials hardening,” Proceedings of the IAEA Technical Meeting on Fuel Behaviour and Modelling Under Severe Transient and LOCA Conditions, IAEA-TECDOC-CD-1709, Mito-city Ibaraki-ken, Japan, October 18-21, 2011, pp. 253-265.

[65] Turque, I., Le Saux, M., Brachet, J.C., Crépin, J., André, G. and Toffolon-Masclet, C., “Metallurgical evolution of a highly hydrided zirconium alloy upon cooling from high temperature,” *Proceedings of the Minerals, Metals and Materials Society 2015 144th Annual Meeting & Exhibition*, Orlando, USA, March 15-19, 2015.

[66] Pshenichnikov, A., Stuckert, J., Walter, M. and Litvinov, D “Hydrides and fracture of pure zirconium and Zircaloy-4 hydrogenated at temperatures typical for loss-of-coolant accident conditions,” *Proceedings of the 23rd International Conference on Nuclear Engineering (ICONE-23)*, Chiba, Japan, May 17-21, 2015.

[67] Brachet, J.C., Toffolon-Masclet, C., Hamon, D., Guilbert, T., Trego, G., Jourdan, J., Stern, A. and Raepsaet, C., “Oxygen, Hydrogen and Main Alloying Chemical Elements Partitioning Upon Alpha-Beta Phase Transformation in Zirconium Alloys,” *Solid State Phenomena*, Vol. 172-174, 2011, pp. 753-759.

[68] Leech, N.A. and Garlick, A., “The influence of environment on the formation of fluting microstructures during fracture of Zircaloy,” Journal of Nuclear Materials, Vol. 125, 1984, pp. 19-24.

[69] Yamanaka, S., Yamada, K., Kurosaki, K., Uno, M., Takeda, K., Anada, H., Matsuda, T. and Kobayashi, S. “Analysis of the electronic structure of zirconium hydride,” *Journal of Alloys and Compounds,* Vol. 330-332, 2002, pp. 313-317.

[70] Yamanaka, S., Setoyama, D., Muta, H., Uno, M., Kuroda, M., Takeda, K. and Matsuda, T., “Characteristics of zirconium hydrogen solid solution,” *Journal of Alloys and Compounds*, Vol. 372, 2004, pp. 129-135.

[71] Lynch, S., “Hydrogen embrittlement phenomena and mechanisms,” *Corrosion Reviews*, Vol. 30, No. 3-4, 2012, pp. 105-123.

[72] Rupa, N., Clavel, M., Bouffioux, P., Domain, C. and Legris, A., “About the mechanisms governing the hydrogen effect on viscoplasticity of unirradiated fully annealed Zircaloy-4 sheet,” *Zirconium in the Nuclear Industry : Thirteenth International Symposium, ASTM STP 1423*, G.D. Moan and P. Rudling, Eds., ASTM International, West Conshohocken, PA, 2002, pp. 811-834.

[73] Le Saux, M., Besson, J., Carassou, S., Poussard, C. and Averty, X., “Behavior and failure of uniformly hydrided Zircaloy-4 fuel claddings between 25°C and 480°C under various stress states, including RIA loading conditions,” *Engineering Failure Analysis,* Vol. 17, No. 3, 2010, pp. 683-700.

[74] Grange, M., Besson, J. and Andrieu, E., “Anisotropic behavior and rupture of hydrided Zircaloy-4 sheets,” *Metallurgical and Materials Transactions A,* Vol. 31, 2000, pp. 679-690.

Figure captions

FIG. 1—*Optical micrographs of transverse cross-sections of creep tested model α_{Zr}(O) samples containing in average (a) 2 wt.% and (b) 4.3 wt.% of oxygen (outer surface on the left); DR: radial direction; DA: tube axis; DT: circumferential direction.*

FIG. 2—*Oxygen and niobium concentration profiles (EPMA) across the thickness of model α_{Zr}(O) samples containing in average (a) 2 wt.% and (b) 4.3 wt.% of oxygen.*

FIG. 3—*Measured (EPMA) and calculated (Thermocalc + Zircobase) α_{Zr}(O) phase volume fraction as a function of oxygen content and temperature.*

FIG. 4—*Pole figures {10.0}, {11.0} and {00.1} recalculated for a model α_{Zr}(O) sample containing 2 wt.% of oxygen in average: (a) surface analysis by EBSD, (b) volume analysis by neutron diffraction; DR: radial direction; DT: circumferential direction.*

FIG. 5—*Strain rate as a function of stress: experimental data on model α_{Zr}(O) samples and predictions of the viscoplastic flow model presented in this paper.*

FIG. 6—*Effect of oxygen on the creep strain rate at 1000°C under 2 and 20 MPa according the creep law developed for α_{Zr}(O) in the present study and the laws proposed by Burton et al. [10] and Donaldson and Evans [47] for Zircaloy-2, Kaddour et al. [41] and Chow et al. [12] for Zircaloy-4 and Kaddour et al. [41] for M5®.*

FIG. 7—*Strain rate as a function of the grain size in zirconium and its alloys according to creep models associated with diffusional flow (Coble, Nabarro-Herring), dislocation-driven and Harper-Dorn deformation mechanisms at 700°C.*

FIG. 8—*Evolution of the maximal measured axial strain (lower bound of fracture strain) as a function of the oxygen content and test temperature of the α_{Zr}(O) samples tested under tensile creep.*

FIG. 9—*SEM micrographs of the fracture surfaces of α_{Zr}(O) samples containing (a) 2 wt.% of oxygen (right figure: enlarged view inside a dimple) and (b) 3.4 wt.% of oxygen (right figure: enlarged view on a nearly brittle zone) fractured at 1000°C; DR: radial direction; DA: tube axis; DT: circumferential direction.*

FIG. 10—*SEM micrographs of the fracture surfaces of (a) an α_{Zr}(O) sample containing 3.4 wt.% of oxygen fractured at 1100°C (right image: detailed view of α_{Zr}(O) on the tube external periphery) and (b) an α_{Zr}(O) sample containing 5.8 wt.% of oxygen fractured at 1000°C (right image: enlarged view of residual zirconia within the α_{Zr}(O) layer).*

FIG. 11—*Evolution of the creep strain rate during an internal pressure creep test performed on a Zircaloy-4 cladding specimen in steam at 1100°C with a 5 bar internal pressure: experimental result, prediction of the creep model presented in [41] for a non-oxidized cladding and results of finite element simulations considering two or three layers.*

FIG. 12—*(a) Optical micrograph of a transverse cross-section right after hydrogen-charging at 800°C (and cooling at a few °C/min) of a Zircaloy-4 sample containing about 3200 wt.ppm of hydrogen (and about 0.2 wt.% of oxygen) and (b) calculated (Thermocalc + Zircobase) evolution of equilibrium phases volume fractions for Zircaloy-4 containing 3000 wt.ppm of hydrogen (and 0.14 wt.% of oxygen) as a function of temperature.*

FIG. 13—*Specimen used for axial tensile tests on (prior-) β_{Zr} materials (dimensions in mm).*

FIG. 14—*Evolution as a function of temperature of the Young's modulus (accuracy of about ±10 GPa) of model (prior-) β_{Zr} materials, non-hydrided or containing between 1710 and 3220 wt.ppm of hydrogen (and at least 0.2 wt.% of oxygen).*

FIG. 15—*Examples of engineering stress-strain (deduced from cross-head displacement) curves obtained (a) at 135 and 350°C and (b) at 500 and 700°C for model (prior-) β_{Zr} materials, non-*

hydrided or containing between 1710 and 3220 wt.ppm of hydrogen (and at least 0.2 wt.% of oxygen).

FIG. 16—*Evolution as a function of temperature of (a) the plastic elongation at failure and (b) the reduction of area at fracture (accuracy of about ±0.08) obtained for model (prior-)* β_{Zr} *materials, non-hydrided or containing between 1710 and 3220 wt.ppm of hydrogen (and at least 0.2 wt.% of oxygen).*

FIG. 17—*Evolution as a function of temperature of (a) the yield stress at 0.2% plastic strain and (b) the ultimate (maximum) stress obtained for model (prior-)* β_{Zr} *materials, non-hydrided or containing between 1710 and 3220 wt.ppm of hydrogen (and at least 0.2 wt.% of oxygen).*

FIG. 18—*Ductile or brittle fracture modes of the (prior-)* β_{Zr} *phase as a function of temperature and mean hydrogen content; data from this study and from Brachet et al. [3], Stern et al. [14], Cabrera [63], Stuckert et al. [62] and Pshenichnikov et al. [38] (features given in Table 3).*

FIG. 19—*SEM micrographs of the fracture surfaces of model (prior-)* β_{Zr} *samples, non-hydrided or containing 2000 to 3000 wt.ppm of hydrogen (and at least 0.2 wt.% of oxygen), fractured at 135 and 500°C.*

FIG. 20—*Evolution as a function of temperature of the uniform elongation (plastic strain at the maximum stress when failure occurs after necking) obtained for model (prior-)* β_{Zr} *materials, non-hydrided or containing between 1710 and 3220 wt.ppm of hydrogen (and at least 0.2 wt.% of oxygen).*